**Box 1.11 Franck–Condon Factors for Displaced and Distorted Oscillators**

A vibration is said to arise from a *displaced oscillator* when the electronic transition causes a change $\Delta Q$ in the equilibrium bond length, while the angular frequency remains constant ($\Delta\omega = 0$) (Figure B1.11.1). The Franck–Condon factor $F(E)$ for a displaced oscillator is given by

$$F(E) = \frac{S^m e^{-S}}{m!} \tag{B1.11.1}$$

where the vibrational quantum $m$, the vibrational energy $\hbar\omega$, and the energy difference E between the overlapping vibrational wavefunctions are related by $m = E/\hbar\omega$. A typical example of a displaced oscillator is the carbon–carbon stretching vibration with a vibrational energy of about 1200 $cm^{-1}$.

When the electronic transition causes a change in the angular frequency $\Delta\omega$ and the equilibrium distance remains the same ($\Delta Q = 0$), vibration is said to arise from a *distorted oscillator*. The carbon-hydrogen stretching vibration with 3000 $cm^{-1}$ is an example for a distorted oscillator. The Franck–Condon factor for a distorted oscillator is

$$F(E) = \frac{2\sqrt{\omega_i\omega_f}}{\omega_i + \omega_f}\left(\frac{\Delta\omega}{\omega_i + \omega_f}\right)^m \frac{1 \cdot 3 \cdot 5, \ldots, (m-1)}{2 \cdot 4, \ldots, m} \tag{B1.11.2}$$

for $m$ = even, and it is $F(E) = 0$ for $m$ = odd.

There are also expressions for the general, displaced *and* distorted case and for the degenerate case, which can be found in Ref. [111]. Evidently, the evolution of the Franck–Condon factors with energy differs for displaced and distorted oscillators. They cross at about 4000 $cm^{-1}$. Below 4000 $cm^{-1}$, the FC factor for displaced oscillators is larger, above that for distorted oscillators.

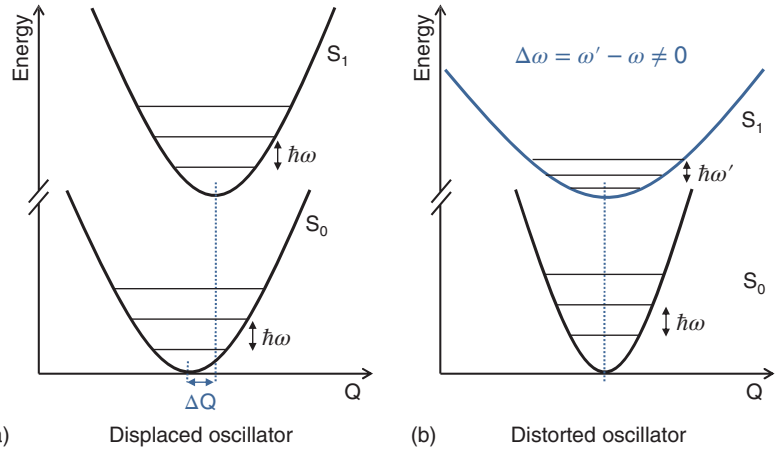


**Figure B1.11.1** Illustration of the potential energy for (a) a displaced oscillator and (b) a distorted oscillator.

Further, from Eq. (1.15), one can see that $S$ is a measure of the ratio between the potential energy associated with a vibrational excitation, $k\Delta Q^2/2$, and the energy of the vibrational quanta, $\hbar\omega_m$. The Huang–Rhys parameter can thus be considered to yield the number of quanta involved in the vibrational excitation. Upon absorption of a photon, the molecule is at first still at the equilibrium position of the ground state, $Q_{GS}$, and has excess potential energy with respect to the equilibrium position of the excited state, $Q_{ES}$. This excess energy is released by the emission of vibrational quanta when the nuclei adapt to the change in electronic charge distribution. It is referred to as *geometric reorganization energy* or *relaxation energy* and is given by

$$E_{rel} = S\hbar\omega \text{ for a single mode, and} \tag{1.22a}$$

$$E_{rel} = \sum_i S_i\hbar\omega_i \text{ for several modes } i \tag{1.22b}$$

The same reorganization energy is released following the emission of a photon when the molecule returns from the excited-state geometry to the ground-state geometry. This is indicated in Figure 1.24.

#### 1.4.2.3 The Spin Factor

The final term to consider in determining the rate of a transition according to Eq. (1.8) is the spin wavefunction $\Psi_{spin}(\alpha_i, \beta_i)$, i.e. the value of the integral $\langle\Psi_{spin,i}|\Psi_{spin,f}\rangle$. This integral takes only two values, i.e. 0 if the spins of initial and final state differ, and 1 if they are equal. Thus, transitions between singlet states or between triplet states, such as $S_1 \leftarrow S_0$ or $T_n \leftarrow T_1$, are *spin-allowed*, yet transitions from triplet to singlet states or vice versa, such as $T_1 \rightarrow S_0$, are *spin-forbidden*. Nevertheless, luminescence arising from the $T_1 \rightarrow S_0$ transition is experimentally observed,

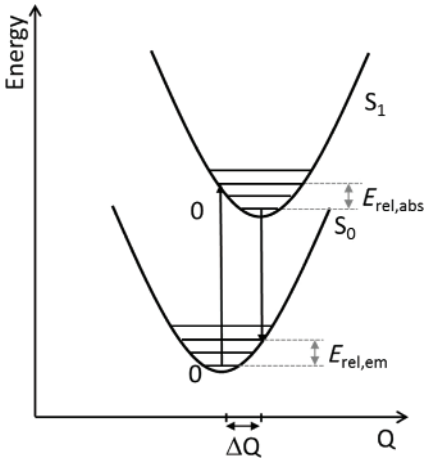


**Figure 1.24** Potential energy diagram showing the relaxation energies $E_{\mathrm{rel,abs}}$ and $E_{\mathrm{rel,em}}$ associated with the process of absorption and emission, respectively.

and it is referred to as *phosphorescence* to distinguish it from the $S_1 \rightarrow S_0$ transition, the *fluorescence*.

How does such a spin-forbidden transition acquire a finite transition rate? This is only possible if, by some perturbation, the triplet state wavefunction obtains some contribution from a singlet state wavefunction and vice versa. The transition then takes place between the singlet admixture in the triplet excited-state wavefunction and the singlet ground state, and the triplet state admixture in the triplet ground-state wavefunction and the triplet excited state (Figure 1.25).

Such a perturbation is provided by the mechanism of spin-orbit coupling. If the spin angular momentum is $\sigma$ and the orbital angular momentum is $l$ of an electron couple, then a change in spin angular momentum can be compensated by an opposite change in orbital angular momentum since only the total angular momentum $j = l + \sigma$ needs to

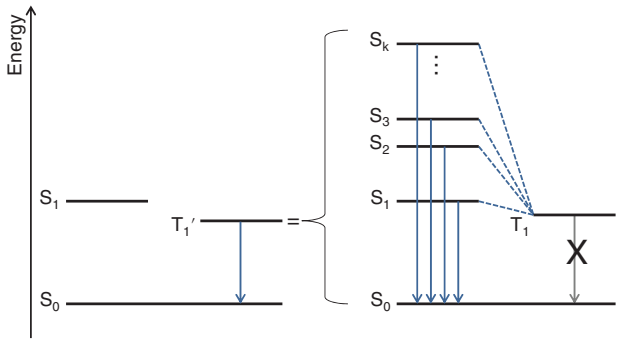


**Figure 1.25** State diagram illustrating how a nominal triplet state $T_1'$ acquires oscillator strength for the actually spin-forbidden $T_1' \rightarrow S_0$ transition through admixtures of the singlet states $S_1 - S_k$ into the pure triplet state $T_1$.

be conserved during the optical transition. For example, a spin flip of an electron can occur when it is accompanied by a change in the associated angular momentum from $l_y$ to $l_x$. If the energy associated with the spin-orbit coupling is small compared to the total energy of the molecule, the effect of spin-orbit coupling on the wavefunction of a state can be described in the framework of perturbation theory. Let ${}^3\Psi_1^0 := {}^3(\Psi_{\mathrm{el}}\Psi_{\mathrm{spin}})_1^0$ denote the wavefunction of a pure triplet excited state, ${}^1\Psi_0^0$ be the wavefunction of a pure singlet ground state, ${}^1\Psi_{\mathrm{k}}^0$ the pure $k^{\mathrm{th}}$ singlet excited state, and $\hat{H}_{\mathrm{SO}}$ be the Hamiltonian of the perturbing spin-orbit interaction. The pure triplet excited state ${}^3\Psi_1^0$ will obtain admixtures of higher-lying singlet states ${}^1\Psi_{\mathrm{k}}^0$. The amount of their contributions depends on how well they overlap with the pure triplet state (after the spin-orbit coupling has happened), and how far the two states are separated in energy. Mathematically, this is expressed as

$$\left|{}^3\Psi_1'\right\rangle = \left|{}^3\Psi_1^0\right\rangle + \sum_k \frac{\left\langle {}^1\Psi_{\mathrm{k}}^0 \middle| \hat{H}_{\mathrm{SO}} \middle| {}^3\Psi_1^0 \right\rangle}{E(T_1) - E(S_k)} \left|{}^1\Psi_{\mathrm{k}}^0\right\rangle \quad (1.23)$$

with ${}^3\Psi_1'$ denoting the perturbed triplet state. An analogous expression can be written for the singlet ground state as follows:

$$\left|{}^1\Psi_0'\right\rangle = \left|{}^1\Psi_0^0\right\rangle + \sum_k \frac{\left\langle {}^3\Psi_{\mathrm{k}}^0 \middle| \hat{H}_{\mathrm{SO}} \middle| {}^1\Psi_0^0 \right\rangle}{E(S_0) - E(T_k)} \left|{}^3\Psi_{\mathrm{k}}^0\right\rangle \quad (1.24)$$

Due to the large energy separation between the singlet ground state and higher-lying triplet states, the triplet admixture in the singlet ground-state wavefunction is small. To obtain the rate for the transition, the wavefunctions of the perturbed triplet excited state and singlet ground state are inserted into Fermi's golden rule (Eq. (1.6)), as follows:

$$\begin{aligned} k_{\mathrm{if}} &= \frac{2\pi}{\hbar}\rho \left| \left\langle {}^3\Psi_1' | e\hat{\mathbf{r}} | {}^1\Psi_0' \right\rangle \right|^2 \\ &= \frac{2\pi}{\hbar}\rho (A + B + C + D)^2 \quad \text{with} \end{aligned} \quad (1.25)$$

$$A = \left\langle {}^3\Psi_1^0 | e\hat{\mathbf{r}} | {}^1\Psi_0^0 \right\rangle$$

$$B = \sum_k \frac{\left\langle {}^1\Psi_{\mathrm{k}}^0 | \hat{H}_{\mathrm{SO}} | {}^3\Psi_1^0 \right\rangle}{E(T_1) - E(S_k)} \left\langle {}^1\Psi_{\mathrm{k}}^0 | e\hat{\mathbf{r}} | {}^1\Psi_0^0 \right\rangle$$

$$C = \sum_k \frac{\left\langle {}^3\Psi_{\mathrm{k}}^0 | \hat{H}_{\mathrm{SO}} | {}^1\Psi_0^0 \right\rangle}{E(S_0) - E(T_k)} \left\langle {}^3\Psi_1^0 | e\hat{\mathbf{r}} | {}^3\Psi_{\mathrm{k}}^0 \right\rangle$$

$$D = \sum_k \frac{\left\langle {}^1\Psi_{\mathrm{k}}^0 | \hat{H}_{\mathrm{SO}} | {}^3\Psi_1^0 \right\rangle}{E(T_1) - E(S_k)} \sum_j \frac{\left\langle {}^3\Psi_{\mathrm{j}}^0 | \hat{H}_{\mathrm{SO}} | {}^1\Psi_0^0 \right\rangle}{E(S_0) - E(T_j)} \times \left\langle {}^1\Psi_{\mathrm{k}}^0 | e\hat{\mathbf{r}} | {}^3\Psi_{\mathrm{j}}^0 \right\rangle$$

Remembering that our wavefunction contains both the spatial and the spin wavefunction, it is evident that terms A and D vanish as they contain a product of orthogonal spins. The remaining contributing terms are B and C, with C being only a minor contribution due to the large energy difference between $S_0$ and $T_k$, compared to that between $T_1$ and $S_k$.

This illustrates how the intensity of phosphorescence results mainly from the admixture of singlet wavefunctions in the nominal triplet state. Detailed quantum mechanical studies have been performed for the polyacenes [112]. It turns out that the spin-orbit coupling admixes states of the same parity, yet of different symmetry. As a result of spin-orbit coupling, the triplet state can have a different polarization to the singlet state. This has been observed not only for molecules such as naphthalene, phenanthrene, chrysene, picenene, and coronene [112] but also for polymers such as a Pt-containing phenylene ethynylene [113] and polyfluorene [114].

The amount of the singlet admixture to the nominal triplet state depends not just on the energy separation between $T_1$ and $S_k$ but also on the magnitude of the spin-orbit coupling. For atoms, one can show that the perturbing Hamiltonian $\hat{H}_{SO}$ is proportional to the fourth power of the atomic charge, $\hat{H}_{SO} \propto Z^4/n^3(l+1)(l+0.5)l$, with n and l being the quantum numbers, and for molecules, a similar expression exists with a dependence between the fourth and fifth power of the atomic charge. As a result, strong phosphorescence is observed when atoms with a high mass are incorporated in the chromophore, as is the case for the organometallic complexes such as the Ir complexes used for phosphorescent OLEDs (see Figure 4.9 in Chapter 4), or for halogen-substituted polyacenes (*internal heavy atom effect*) (Figure 1.26), as illustrated in Table 1.4. Sometimes, sufficient interaction between orbitals can even be obtained if the heavy atom is placed immediately next to an organic chromophore, for example by using a brome or iodine-containing solvent in solution [117, 118], or by having some metal like Pd present in the film as a residue from the metal-catalyzed synthesis [115]. This is referred to as *external heavy atom effect*.

Even in the absence of heavy metals, phosphorescence can still occur, albeit at much weaker intensity. In a semiclassical picture, one can attribute this to the fact that only the sum $j = s + l$ of spin $s$ and orbital angular momentum $l$ needs to be preserved. If the orbital angular momentum changes as a result of vibrations, the spin can flip. In a quantum mechanical picture, the torsions provide the perturbation to mix orbitals with different angular momentum such as σ and π [116, 119, 120]. Vibrationally induced spin-orbit coupling is an example where the Born–Oppenheimer approximation no longer provides a suitable description. Overall, vibrationally induced spin-orbit coupling is weak compared to heavy-metal–induced spin-orbit coupling. As a result, radiative rates for phosphorescence are in the range of $10^6\ s^{-1}$ for organometallic complexes, yet reach only $1\ s^{-1}$ for purely organic compounds.

In summary, from the Fermi's golden rule expression, Eq. (1.6) follows that a high rate of absorption and emission requires two states that are of the same parity and spin, with frontier orbitals that contain a well-delocalized, well-overlapping π-electron system. Transitions with reduced orbital overlap between the initial and final state, such as charge-transfer-type transitions, have a concomitantly reduced intensity. There are no transitions between states of different parity. The intensity of the transition between singlet and triplet states depends on the strength of the spin-orbit coupling. The spectral shape of the transition is modulated by the FC factor.

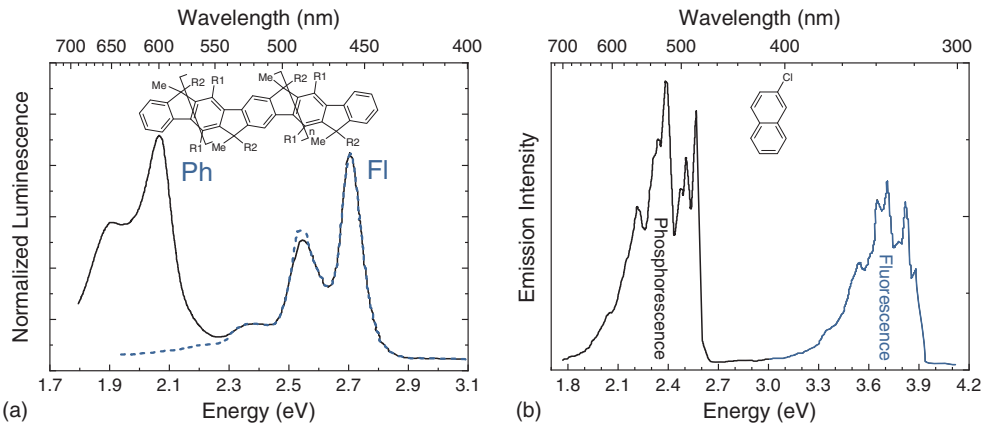


**Figure 1.26** (a) Luminescence of MeLPPP at room temperature for optical excitation (dotted line) showing only fluorescence (Fl) and for electrical excitation (solid line), displaying both fluorescence and phosphorescence (Ph). The phosphorescence observed for electrical excitation is enhanced by the presence of palladium in the film. (After [115].) (b) Fluorescence and phosphorescence of Cl-substituted naphthalene, taken in Me-THF at 77 K. (From [116].)

### 1.4.3 A Classical Picture of Light Absorption

In addition to the quantum mechanical description of light absorption presented in Section 1.4.2, it is useful to be aware of the corresponding classical picture that leads to the macroscopic quantities such as the refractive index and absorption coefficient. Further, it is instructive to see how the quantum mechanical description and the experimental macroscopic measurements on a sample connect.

#### 1.4.3.1 The Lorentz Oscillator Model and the Complex Refractive Index

Classically, the process of light absorption or emission may be understood as a driven, damped oscillation. The changing electromagnetic field of the light wave accelerates the electron distribution in the molecule and causes it to follow the field almost instantly. As with any driven oscillation, the transfer of energy from the driving electromagnetic field to the oscillating electron cloud is at maximum when the frequency of light wave matches the resonance frequency $\omega_0$ of the electron distribution. This transfer of energy corresponds to the absorption of a photon.

The mathematical formalism is straightforward if one is familiar with the driven damped oscillator and is known as the Lorentz oscillator model. We shall sketch it briefly and for simplicity consider a single electron of mass $m$ and charge $e$ that is bound to an atom by an elastic force with spring constant $k$. It has a resonance frequency of oscillation ${\omega_0}^2 = k/m$. The electromagnetic field of the light exerts a force $F_{\mathrm{EM}}$ on the electron,

$$F_{\mathrm{EM}} = e\boldsymbol{E} + e\boldsymbol{v} \times \boldsymbol{B} \tag{1.26}$$

where $\boldsymbol{E}$ and $\boldsymbol{B}$ are the electric and magnetic field, respectively, and $\boldsymbol{v}$ is the velocity of the electron. In this expression, the second, magnetic term is small compared to the first, electric term and can thus be neglected. Considering one-dimensional motion and using $E(t) = E_0 e^{-i\omega t}$ for the oscillating electric field yields

$$F_{\mathrm{EM}} \cong eE_0 e^{-i\omega t} \tag{1.27}$$

for the force that accelerates the electron with an acceleration $\ddot{x}$. The electron resists the resulting motion through its inertia with $F_{\mathrm{inert}} = -m\ddot{x}$, and it is held back by the elastic restoring force that binds it to the atom, $F_{\mathrm{spring}} = -kx$. $x$ is the displacement of the electron from its original position. The whole motion is usually damped by a force that is proportional to the velocity $\dot{x}$ of the object and to its mass. This proportionality is expressed by a phenomenological damping constant $\gamma$, so $F_{\mathrm{damp}} = \gamma m\dot{x}$. It is equivalent to friction in a mechanical system. In the present case, damping arises from the coupling of the object to its environment. Equating the forces acting on the electron

$$F_{\mathrm{inert}} + F_{\mathrm{damp}} + F_{\mathrm{spring}} = -F_{\mathrm{EM}} \tag{1.28}$$

yields the equation of motion

$$m\ddot{x} - \gamma m\dot{x} + kx = eE_0 e^{-i\omega t} \tag{1.29}$$

This equation describes how the electron follows the field in an oscillatory motion. The general solution to this equation is

$$x(t) = x_{\mathrm{trans}}(t)e^{-t\gamma/2} + x_0 e^{-i\omega t} \tag{1.30}$$

with $x_{\mathrm{trans}}(t) = x_{t0} \exp\left[-i\sqrt{\left({\omega_0}^2 - \gamma^2/4\right)}t\right]$. The first term, $x_{\mathrm{trans}}(t)e^{-t\gamma/2}$, represents a damped oscillation of frequency $({\omega_0}^2 - \gamma^2/4)$ that disappears for $t > \gamma^{-1}$. After this transient feature, the electron follows the oscillation of the electromagnetic field. The amplitude of the electron's displacement can be found by inserting Eq. (1.30) into Eq. (1.29) for $t > \gamma^{-1}$. It is

$$x_0 = \frac{eE_0}{m}\frac{1}{\left({\omega_0}^2 - \omega^2\right) - i\omega\gamma} \tag{1.31}$$

What is this classical model good for? It turns out that this simple picture of an electron forced into oscillations by a periodically changing electric field vector can be helpful to develop an intuitive understanding of the quantum mechanical process of light absorption. For a quantitative description, correction terms are needed that are beyond the scope of this book. They can be found in Ref. [121].

Consider, for example, the quantum mechanical selection rule that says light absorption (or emission) must be accompanied by a change in angular momentum by one unit. This can be readily rationalized in this oscillator model (Figure 1.27). The incident oscillating electromagnetic field vector causes the electron cloud to follow and thus to redistribute. Instead of the symmetric charge distribution that was there before the action of the electromagnetic field, there is now an oscillating, polar charge distribution. Looking at the time average, there is an additional node. In a single-electron atom such as hydrogen, the electron distribution may change from one corresponding initially to a 1s orbital to one corresponding to a 2p orbital. In a molecule, the distribution may change from a $\pi$ to a $\pi^*$ orbital. This additional node, induced by the oscillating field, corresponds to a unit change in angular momentum upon absorption of a photon.

In a classical picture, an oscillating charge distribution implies that there is an electromagnetic dipole, just like in the simple antenna of an ordinary household radio receiver. The magnitude of the dipole moment scales with the amount of charge that oscillates and the distance over which it oscillates. This dipole is induced by the incident electromagnetic wave. It is referred to as *transition dipole* $\mu$ since it is associated with the optical transition, and, for a single oscillating electron, it is given by

$$\mu = ex_0 \tag{1.32}$$

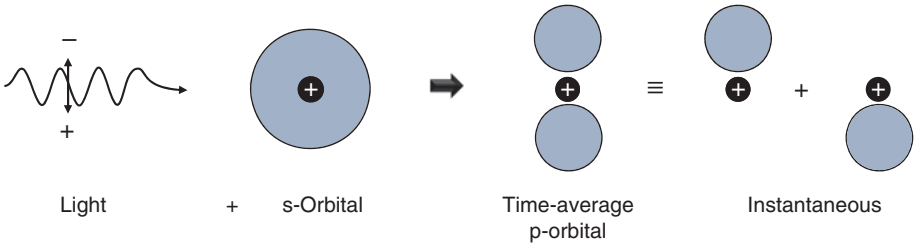


**Figure 1.27** Light absorption in the framework of the Lorentz oscillator model. The oscillating electric field vector of the incident electromagnetic light wave causes the electron cloud of the atom to follow in resonance. The time-averaged charge distribution thus changes from an initially spherical shape to one with large probabilities at the turn-around points of the oscillation, and a low one in the middle. In this example, light absorption introduces a node by changing the time-averaged charge distribution from an s-orbital to a p-orbital. (After [116].)

The dipole moment per unit field strength that can be induced in an atom or molecule defines the *polarizability* $\alpha$ of the atom or molecule,

$$\alpha = \mu / E_0 \tag{1.33}$$

It gives a measure of the ease by which an electric field can distort the electron distribution of the molecule. Keep in mind that, in general, the force due to an electric field is opposed by the elastic restoring force, $eE_0 = -kx_0$. Using Eqs. (1.32) and (1.33), one can see that the restoring force constant is inversely proportional to the polarizability, $k = e^2/\alpha$.

In the framework of this classical picture, the frequency dependence of the refractive index of a molecule and of its absorption coefficient can be derived. We shall outline the essential steps.

In a macroscopic sample, there is not just one oscillating dipole but $N$ of them per unit volume. This gives a dipole moment per unit volume, i.e. a macroscopic polarization density $P$,

$$P = N\mu = N\alpha E_0 = N\frac{ex_0}{E_0}E_0 = \frac{Ne^2}{m}\frac{1}{\left({\omega_0}^2 - \omega^2\right) - i\omega\gamma}E_0 \tag{1.34}$$

The overall electric field inside a macroscopic sample then is given by a superposition of the electromagnetic field inside the sample and of the induced dipole field. As it involves displaced charges, it is referred to as *dielectric displacement field* D

$$D = \varepsilon_0 E_0 + P \tag{1.35}$$

Using Eq. (1.34), this can be expressed as

$$D = \varepsilon_0\left(1 + \frac{Ne^2}{\varepsilon_0 m}\frac{1}{\left({\omega_0}^2 - \omega^2\right) - i\omega\gamma}\right)E_0 \tag{1.36}$$

The term in the bracket is the *dielectric constant* $\varepsilon(\omega)$ of the macroscopic sample. It describes how the field present in the macroscopic sample is altered due to the fact that the electron distributions of the molecules interact with the electromagnetic light wave. From this derivation, it should be evident that the dielectric constant is the macroscopic equivalent of the polarizability $\alpha$.

$$\varepsilon(\omega) = 1 + \frac{Ne^2}{\varepsilon_0 m}\frac{1}{\left({\omega_0}^2 - \omega^2\right) - i\omega\gamma} \tag{1.37}$$

Maxwell has shown that the dielectric constant of a nonmagnetic material relates to its refractive index as $\tilde{n}^2 = \varepsilon(\omega)$. Here, the dielectric constant is a complex number, and thus the refractive index is also a complex number, indicated here by a tilde over the symbol. What does a complex refractive index mean? If one writes

$$\tilde{n} = n - i\kappa \tag{1.38}$$

and uses this to describe the propagation of an electromagnetic wave in matter

$$E = E_0 \exp[i(\omega t - \tilde{n}k_0 z)] = E_0 \exp[-\kappa k_0 z]\exp[i(\omega t - nk_0 z)] \tag{1.39}$$

one can immediately see that $\kappa$ relates directly to the absorption coefficient (see Eq. (1.10)) as $\alpha = 2\kappa k_0$ since the intensity relates to the amplitude of a wave as $I = E^2$. Thus, $\kappa$ is responsible for an attenuation of the propagating wave. $n$ is simply the usual, real refractive index that describes the dispersion of a light wave. For dilute media, not too far away from the resonance frequency $\omega_0$, one can approximate the combination of Eqs. (1.37) and (1.38) to [121, 122]

$$n(\omega) \approx 1 + \frac{Ne^2}{4\varepsilon_0 m}\frac{(\omega_0 - \omega)/\omega}{(\omega_0 - \omega)^2 + (\gamma/2)^2} \quad \text{and}$$
$$\kappa(\omega) \approx \frac{Ne^2}{4\varepsilon_0 m}\frac{\gamma/2\omega}{(\omega_0 - \omega)^2 + (\gamma/2)^2} \tag{1.40}$$

with the frequency dependence as indicated in Figure 1.28. Two features are to be noted.

First, there is a steep change in the refractive index close to the resonance frequency, where absorption is at the maximum. A wavelength dependence of the refractive

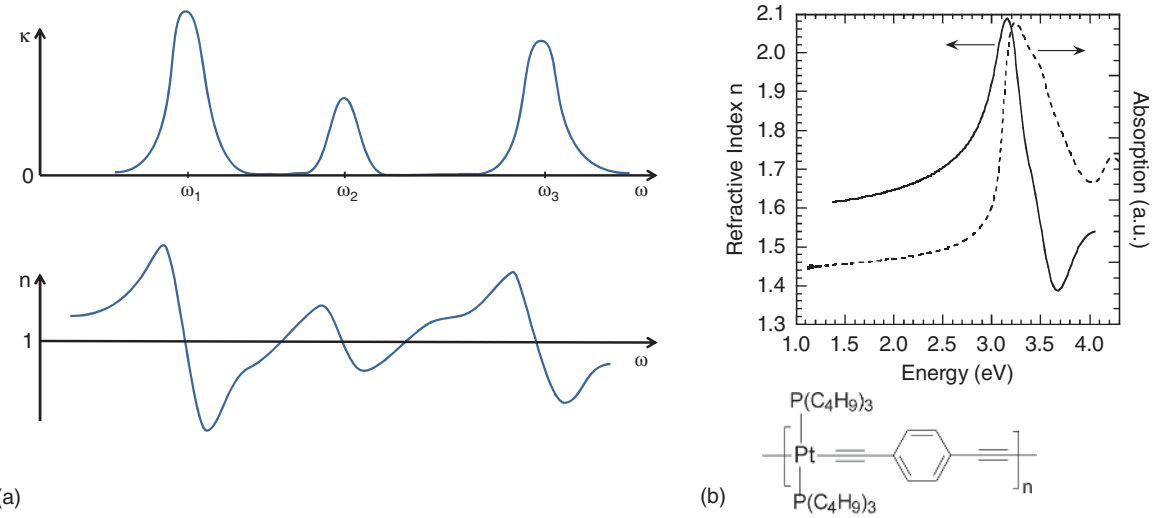


**Figure 1.28** The dependence on the energy $\hbar\omega$ of the incident light for the two components $n$ and $\kappa$ of the complex index of refraction $\tilde{n} = n - i\kappa$. (a) Schematic illustration for three optical transitions at $\omega_1$, $\omega_2$, and $\omega_3$. (b) Measured refractive index and absorption for a Pt-polymer. (After [123].)

index thus needs to be taken into account near the absorption edge, e.g. when modeling the fluorescence spectrum according to Eq. (1.16a and b), while it can be neglected at some distance from the absorption edge, e.g. when modeling phosphorescence.

Second, $\kappa$ is proportional to the classical expression for the power that is transferred from an external driving force to an oscillating object in the framework of the driven damped oscillator. That power is simply $P = F\dot{x}$, i.e. for an incident electromagnetic light wave that interacts with a single electron bound to an atom, $P = eE\dot{x}$. Taking the time average, near the resonance frequency, this approximates to

$$\langle P(\omega)\rangle \approx \frac{e^2E_0^2}{4m}\frac{\gamma/2}{(\omega_0-\omega)^2+(\gamma/2)^2} = \frac{e^2E_0^2\pi}{4m}\mathcal{L}(\omega) \tag{1.41}$$

with

$$\mathcal{L}(\omega) = \frac{1}{\pi}\frac{\gamma/2}{(\omega_0-\omega)^2+(\gamma/2)^2} \tag{1.42}$$

being the Lorentzian curve. It has a full width at half maximum of $\gamma$ and a maximum of $\mathcal{L}(\omega) = 2/\pi\gamma$. Here, we used the normalization $\int_0^\infty \mathcal{L}(\omega)d\omega = 1$.

This Lorentzian lineshape can indeed be observed in molecular transitions, provided that one looks at a single molecule or at a group of molecules that all have exactly the same resonance frequency. The latter can be realized through techniques such as site-selective spectroscopy on molecules embedded in inert glasses and Shpolskii matrices, or through hole-burning spectroscopy. These techniques are discussed in Chapter 2.

#### 1.4.3.2 Relating Experimental and Quantum Mechanical Quantities: The Einstein Coefficients, the Strickler–Berg Expression, and the Oscillator Strength

Experimentally measured quantities such as the absorption coefficient or the emission lifetime can be related to quantum mechanical entities with the help of the Einstein coefficients and the Strickler–Berg relationship. In 1917, Einstein [124] derived the fundamental relationship between the transition probabilities for induced absorption and emission and that for spontaneous emission. His result showed that the spontaneous emission probability is directly proportional to the corresponding absorption probability and to the third power of the frequency of the transition. In the derivation of his equations, it is necessary to assume that the absorption band is sharp and that the fluorescence occurs at the same wavelength as the absorption. This implies that his equations are strictly applicable only to atomic transitions. Strickler and Berg extended his work in 1962 so that it becomes applicable to polyatomic molecules [109, 112]. While the Einstein coefficients are treated in many textbooks on optics, the extension of Strickler and Berg that includes vibrational levels is not commonly summarized at a textbook level, which is why they are included here in a more detailed way. For the practically minded student, it may suffice to merely take note of the gray-shaded equations (Eqs. 1.47, 1.53b, 1.57, 1.62b, 1.65b, 1.67, 1.69).

Consider a large number of chromophores that are embedded in a medium of refractive index $n$ and that are in thermal equilibrium within a cavity of temperature $T$. These chromophores will absorb photons and they will emit photons. Let $N_l$ be the number of chromophores

in the lower state and $N_u$ those in the upper state, and $h\nu$ be the energy separating the two states. For a given frequency $\nu$, the energy density of radiation (in $10^{-7}$ J cm$^{-3}$ per unit frequency range $d\nu$) within the medium is given by Planck's black-body law

$$u(\nu) = \frac{8\pi h\nu^3 n^3}{c^3}\left(e^{\frac{h\nu}{kT}} - 1\right)^{-1} \tag{1.43}$$

Let us now introduce a probability coefficient for transitions between a lower electronic state $l$ with vibrational level $w$ and an upper electronic state $u$ with vibrational level $m$. For spontaneous emission, this shall be $A_{uw\to lm}$ (the *Einstein A coefficient*), for stimulated emission, this shall be $B_{uw\to lm}$ and for absorption, we use $B_{lm\to uw}$ (the *Einstein B coefficient*). The frequency of the transition is $\nu = \nu_{uw\to lm} = \nu_{lm\to uw}$. Spontaneous emission is a random process that determines the normal radiative lifetime of an excited state. In contrast, stimulated emission or absorption occurs when an incident photon induces the transition between the two states. Thus, the rate $\Delta N$ for chromophores going from one state to the other by spontaneous emission depends only on the number of chromophores present in the initial state, while for stimulated emission and absorption, it also depends on the energy density of the radiation. The rate for molecules going from the lower state to the upper state by absorption is then [109]

$$\Delta N_{lm\to uw} = N_{lm}B_{lm\to uw}u(\nu) \tag{1.44}$$

while the rate for molecules going in the opposite direction by emission is

$$\Delta N_{uw\to lm} = N_{uw}[B_{uw\to lm}u(\nu) + A_{uw\to lm}] \tag{1.45}$$

Einstein showed that $B_{uw\to lm}$=$B_{lm\to uw}$. Furthermore, the populations of lower and upper states are related by the Boltzmann distribution, as follows:

$$N_{uw} = N_{lm}\exp\left(-\frac{h\nu}{kT}\right) \tag{1.46}$$

In thermal equilibrium, the expressions of Eqs. (1.44) and (1.45) must be equal. Considering this and inserting Eqs. (1.43) and (1.46) yields the *Einstein relation*, as follows:

$$A_{uw\to lm} = 8\pi h\left(\frac{\nu n}{c}\right)^3 B_{lm\to uw} \tag{1.47}$$

The feature to notice is that in between the probability of spontaneous emission, given by the Einstein A coefficient, and the probability of absorption, given by the Einstein B coefficient, there is the cube of the transition energy that arises from the photon density of states.

How do these coefficients relate to experimentally measured quantities? $u(\nu)/h\nu$ is the photon density in a frequency range $d\nu$. When a beam of photon density $u(\nu)/h\nu$ passes through a material, photons are absorbed so that the photon density changes by

$$\frac{\mathrm{d}u(\nu)}{h\nu} = -\sigma'\frac{N_{lm}}{A}\frac{u(\nu)}{h\nu} \tag{1.48}$$

where $\frac{N_{lm}}{A}$ is the number of absorbing chromophores per area (in cm$^2$) and $\sigma'$ is the absorption cross section of a chromophore (in cm$^2$). The absorption results in a number of excited chromophores $\Delta N_{lm\to uw}$ per second, i.e.

$$\Delta N_{lm\to uw} = -c_n\frac{du(\nu)}{h\nu}\cdot A = \frac{c}{n}\sigma' N_{lm}\frac{u(\nu)}{h\nu} \tag{1.49}$$

with $c_n = c/n$ being the velocity of the light wave. One obtains the excitation rate per unit volume over the entire vibronic band by integration over the entire frequency range from the 0th to the w$^{\text{th}}$ vibrational level of the upper state, i.e. from $\nu_{l0\to u0}$ to $\nu_{l0\to uw}$.

$$\Delta N_{l0\to u} = N_{l0}\frac{c}{hn}\int_{\nu_{l0\to u0}}^{\nu_{l0\to uw}}\frac{\sigma'(\nu)u(\nu)}{\nu}d\nu \tag{1.50}$$

If one assumes that the energy density is approximately constant in this range, one can write this as

$$\Delta N_{l0\to u} = N_{l0}\left[\frac{c}{hn}\int_{\nu_{l0\to u0}}^{\nu_{l0\to uw}}\frac{\sigma'(\nu)}{\nu}d\nu\right]u(\nu) \tag{1.51}$$

which, by comparison with Eq. (1.44), immediately yields

$$B_{l0\to u} = \sum_w B_{l0\to uw} = \frac{c}{hn}\int\frac{\sigma'(\nu)}{\nu}d\nu \tag{1.52}$$

where the integral covers the frequency range of the entire vibronic band. Instead of the absorption cross section, it is more practical to use the decadic molar extinction coefficient $\left(\text{in } \frac{\text{cm}^2}{\text{mol}}, \text{Eq. (1.13)}\right)$ so that

$$B_{l0\to u} = \frac{2303}{N_A}\frac{c}{hn}\int\frac{\varepsilon(\nu)}{\nu}d\nu \tag{1.53a}$$

$$B_{l0\to u} = 3.82 * 10^{-21}(\text{mol})\frac{c}{hn}\int\frac{\varepsilon(\nu)}{\nu}d\nu \tag{1.53b}$$

where $N_A$ denotes Avogadro's constant. Since $N_A$ is in units of mol$^{-1}$, in Eq. (1.53b), the unit mol is still part of the expression. Eq. (1.53) relates the Einstein B coefficient for absorption to a quantity that can be measured experimentally in a simple way. The absorption occurs from the 0th vibrational level of the lower state to all vibrational levels of the upper state.

For compounds that show a clear mirror relationship between absorption and emission, one can assume that $\sum_w B_{l0\to uw} = \sum_m B_{u0\to lm}$, and one can then obtain the Einstein A coefficient for spontaneous emission by the Einstein relation, Eq. (1.47), as

$$A_{u0\to l} = \sum_m A_{u0\to lm} = 8\pi h\left(\frac{n}{c}\right)^3\sum_w \nu^3 B_{l0\to uw} \tag{1.54}$$

Note again that $\nu = \nu_{l0\rightarrow uw}$ and $\nu$ therefore depends on the respective transition. Strickler and Berg have further shown that the intrinsic radiative decay rate, $\tau_0$, can be related to the Einstein coefficients in the following way. Since $A_{uw\rightarrow lm}$ is the probability coefficient for spontaneous emission, it follows that it relates to $\tau_0$ as

$$\tau_0^{-1} = A_{u0\rightarrow l} = \sum_m A_{u0\rightarrow lm} \tag{1.55}$$

Their calculations show that

$$\begin{aligned}\frac{1}{\tau_0} &= A_{u0\rightarrow l} = \frac{8\cdot 2303\pi n^2}{c^2 * N_A}\frac{1}{\langle\nu^{-3}\rangle}\int\frac{\varepsilon(\nu)}{\nu}d\nu \\ &= \frac{8\pi h n^3}{c^3}\frac{1}{\langle\nu^{-3}\rangle}B_{l0\rightarrow u}\end{aligned} \tag{1.56}$$

where $\frac{1}{\langle\nu^{-3}\rangle} = \int I(\nu)d\nu / \int \nu^{-3}I(\nu)d\nu$. $I(\nu)$ is the fluorescence intensity measured in number of photons per frequency interval. Instead of using the frequency $\nu = c/\lambda$ in units $s^{-1}$, one may prefer to use wavenumbers $\tilde{\nu} = 1/\lambda$ in units $cm^{-1}$. $c$ and $\lambda$ are the velocity and wavelength of light, respectively. Eq. (1.56) then reads

$$\begin{aligned}A_{u0\rightarrow l} = \frac{1}{\tau_0} &= \frac{8\pi c\cdot 2303}{N_A}\frac{n^2}{\langle\tilde{\nu}^{-3}\rangle}\int\frac{\varepsilon(\tilde{\nu})}{\tilde{\nu}}d\tilde{\nu} \\ &= 2.880 * 10^{-9}\left(\frac{\text{cm}\cdot\text{mol}}{\text{s}}\right)\frac{n^2}{\langle\tilde{\nu}^{-3}\rangle}\int\frac{\varepsilon(\tilde{\nu})}{\tilde{\nu}}d\tilde{\nu}\end{aligned} \tag{1.57}$$

This is the familiar form of the *Strickler–Berg equation* that relates radiative lifetime to the absorption spectrum. If the band is sharp and the absorption and fluorescence occur at the same wavelength, $\tilde{\nu}$ can be considered a constant and can be removed from under the integral. This is the case for most atomic transitions, where Eq. (1.57) reduces to

$$\frac{1}{\tau_0} = 2.880 * 10^{-9}\left(\frac{\text{cm}\cdot\text{mol}}{\text{s}}\right)n^2\tilde{\nu}^2\int\varepsilon(\tilde{\nu})d\tilde{\nu} \tag{1.58}$$

This equation is also useful for order-of-magnitude calculations on molecules.

So far, we have seen how the Einstein coefficients relate to the absorption spectrum and to the radiative lifetime, both being experimentally accessible quantities. It is also possible to relate the Einstein coefficients to the quantum mechanical matrix element for a dipole transition. Let us use the abbreviation $|\boldsymbol{\mu}_{\text{if}}|^2 = |\langle\Psi_{\text{el,i}}|e\hat{\mathbf{r}}|\Psi_{\text{el,f}}\rangle|^2$ for the electronic factor in the Fermi Golden rule expression for a radiative transition. One can see that

$$B_{l0\rightarrow u} = \frac{1}{4\pi\varepsilon_0}\frac{8\pi^3}{3h^2}|\boldsymbol{\mu}_{\text{if}}|^2 = \frac{2\pi^2}{3\varepsilon_0 h^2}|\boldsymbol{\mu}_{\text{if}}|^2 \tag{1.59}$$

where $|\boldsymbol{\mu}_{\text{if}}|^2$ is in SI units. A derivation of this expression (in the CGS system, i.e. without the prefactor $(4\pi\varepsilon_0)^{-1}$) can be found in Appendices 13 and 17 of Ref. [78]. Equating (1.59) with (1.53) yields

$$|\boldsymbol{\mu}_{\text{if}}|^2 = \frac{2303}{N_A}\frac{3\varepsilon_0 ch}{2\pi^2 n}\int\frac{\varepsilon(\nu)}{\nu}\text{d}\nu \tag{1.60}$$

thus directly linking the experimental with the quantum mechanical quantity.

In practice, it has been found convenient to define a measure for the strength of an optical transition. The *oscillator strength* $f$ has been defined as

$$f = (4\pi\varepsilon_0)\cdot\frac{mc}{\pi e^2 n}\int\sigma'(\nu)d\nu = \frac{4\varepsilon_0 mc}{e^2 n}\int\sigma'(\nu)\text{d}\nu \tag{1.61}$$

which can be expressed in terms of the extinction coefficient and wavenumbers using Eq. (1.13)

$$f = \frac{2303}{N_A}\frac{4\varepsilon_0 mc^2}{e^2 n}\int\varepsilon(\tilde{\nu})\text{d}\tilde{\nu} \tag{1.62a}$$

$$f = \frac{4.39 * 10^{-9}}{n}\int\varepsilon(\tilde{\nu})\text{d}\tilde{\nu} \tag{1.62b}$$

The oscillator strength can also be related to the Einstein coefficients. Eq. (1. 52) can be approximated by using an average frequency $\langle\nu\rangle$ to

$$B_{l0\rightarrow u} = \frac{c}{hn}\int\frac{\sigma'(\nu)}{\nu}\text{d}\nu \approx \frac{c}{hn}\frac{1}{\langle\nu\rangle}\int\sigma'(\nu)\text{d}\nu \tag{1.63}$$

Inserting this into Eq. (1.61) yields

$$f = \frac{4\varepsilon_0 mh\langle\nu\rangle}{e^2}B_{l0\rightarrow u} \tag{1.64}$$

Combining this with Eq. (1.59) and using $\langle\nu\rangle = c\langle\tilde{\nu}\rangle$ readily gives

$$f = \frac{8m\pi^2 c\langle\tilde{\nu}\rangle}{3he^2}|\boldsymbol{\mu}_{\text{if}}|^2 \tag{1.65a}$$

$$f = 4.70\cdot 10^{29}\langle\tilde{\nu}\rangle|\boldsymbol{\mu}_{\text{if}}|^2, \text{with } \tilde{\nu} \text{ in } \text{cm}^{-1} \text{ and } \boldsymbol{\mu}_{\text{if}} \text{ in e.s.u, or} \tag{1.65b}$$

$$f = 4.23\cdot 10^{50}(m^{-1}C^{-2})\langle\tilde{\nu}\rangle|\boldsymbol{\mu}_{\text{if}}|^2 \tag{1.65c}$$

if SI units ($\text{m}^{-1}$, $\text{C}\cdot\text{m}$) are used for $\tilde{\nu}$ and $\boldsymbol{\mu}_{\text{if}}$

The oscillator strength was initially introduced in the context of the Lorentz oscillator model. For a classical, single, three-dimensional oscillator, it has its maximum value of 1. Eq. (1.62a and b) can be used to estimate the maximum possible value for the decadic extinction coefficient. The integral can be approximated to

$$\int\varepsilon(\tilde{\nu})d\tilde{\nu} \approx \varepsilon_{\max}\Delta\tilde{\nu} \tag{1.66}$$

where $\varepsilon_{\max}$ is the value of the extinction coefficient at the maximum of absorption and $\Delta\tilde{\nu}$ is the full width at half the maximum height of the absorption band $\varepsilon_{\max}$. Taking

the refractive index to be 1 and a minimum value for $\Delta\tilde{\nu}$ to be 2000 $cm^{-1}$, Eq. (1.62b) gives $1 = 4.39 * 10^{-9} * \varepsilon_{max} * 2000$ $cm^{-1}$ which implies

$$\varepsilon_{max} \approx 10^5 \text{ cm}^{-1} \tag{1.67}$$

In a similar way, the maximum radiative decay rate can be estimated from the oscillator strength. Approximating the radiative lifetime by employing Eq. (1.58), and combining it with Eq. (1.62b) yields

$$\frac{1}{\tau_0} \approx n^3 \tilde{\nu}^2 f \tag{1.68}$$

Using a refractive index of 1, a transition wavelength of 400 nm, i.e. 25 000 $cm^{-1}$, Eq. (1.68) gives an upper limit for the radiative decay rate $k_r = {\tau_0}^{-1} \approx 1 * (2.5 * 10^4)^2 * 1 = 6.25 * 10^8$, i.e. the maximum possible radiative decay rate is on the order of

$$k_{r,max} = 10^9 \text{ s}^{-1} \tag{1.69}$$

We shall add two final remarks. First, we note that in this derivation involving the Einstein coefficients, we have considered the lower and upper state to have the same degeneracy, i.e. both being singlets or both being triplet states. For transitions between singlets and triplets, a degeneracy factor of 3 needs to be taken into account appropriately, i.e. for example, Eq. (1.59) needs to be multiplied by 3 on the right hand side (in general by $\frac{g_u}{g_l}$ where $g_u$ and $g_l$ are the degeneracies of the upper [u] and lower [l] state, respectively) [109].

Second, the definition of the oscillator strength in Eq. (1.61) may seem somewhat arbitrary. It is equivalent to the expression $f = \sigma_{classical}/\sigma_{QM}$, i.e. a definition as the ratio between the absorption cross section $\sigma_{classical}$ of a classical, three-dimensional single-electron oscillator in the Lorentz oscillator model (essentially the expression for $\kappa$ in Eq. (1.38)) and the absorption cross section $\sigma_{QM}$ calculated from the Einstein B coefficient (essentially Eq. (1.52)). When the correct units are used, this leads to the expression given in Eq. (1.61). As the Einstein B coefficient also relates to the quantum mechanical transition dipole operator (Eq. (1.59)), the oscillator strength is a measure for how much a calculated transition rate differs from the maximum possible one that is realized in the model of the three-dimensional single-electron oscillator. A full derivation can be found in Refs. [125–127]. (The latter is a revised version of the earlier manuscript.)

### 1.4.4 Nonradiative Transitions: Internal Conversion and Intersystem Crossing

A nonradiative transition is an *isoenergetic* transition that occurs from the 0th vibrational level of the initial state to a kth vibrational level of the final state. It is usually followed by the fast and irreversible dissipation of vibrational energy to the surroundings (thermal relaxation). The isoenergetic nonradiative transition between two different electronic states is not to be confused with the subsequent vertical thermal relaxation within one electronic state. Whereas the radiative transitions treated in the previous chapter can be indicated in a configuration coordinate diagram by a single vertical arrow, the nonradiative transition is represented by a horizontal arrow (Figure 1.29). The thermal relaxation that follows the nonradiative transition may be indicated by a sequence of vertical arrows.

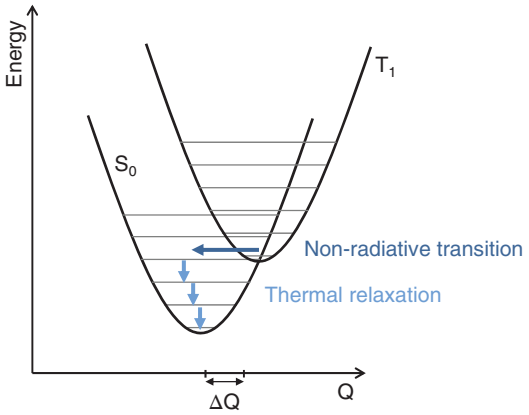


**Figure 1.29** Potential energy diagram illustrating a nonradiative transition from $T_1$ to $S_0$, followed by thermal relaxation.

Nonradiative transitions are referred to as *internal conversion*, with a rate $k_{IC}$, when they take place between states of the same spin manifold (e.g. $S_2 \rightarrow S_1$, $T_2 \rightarrow T_1$) and as *intersystem crossing,* with a rate $k_{ISC}$, when a change of spin is involved (e.g. $S_1 \rightarrow T_1$, $T_1 \rightarrow S_0$). Intersystem crossing from $S_1$ can occur either from the zero-point vibrational level of $S_1$ or from thermally populated vibrational levels of $S_1$. It may take place either into an excited vibrational level of $T_1$ or into a higher excited triplet state $T_2$ (or $T_3$, $T_4$, …) that is closer in energy to $S_1$. Intersystem crossing can also occur in the reverse direction, i.e. from $T_1$ to $S_1$. When the energy difference between the two states is small, thermal activation of $T_1$ to a vibrational level that is isoenergetic with $S_1$ allows for $T_1 \rightarrow S_1$ intersystem crossing. The luminescence that then results from $S_1$ is referred to as thermally activated delayed fluorescence.

The theory of radiationless transitions has been developed in the early 1960s by Siebrand, Robinson, Frosch, Jortner, Englmann, and co-workers, and was found in good agreement with the experimental facts [111, 128–134]. Experimentally, the radiationless transition that has been investigated most extensively is the $T_1 \rightarrow S_0$ transition in aromatic hydrocarbons, notably polyacenes [135–143].

At later times, scientific attention also included the radiationless deactivation of this transition in organometallic complexes [144, 145]. Despite their relevance to the quantum yields of luminescence and photocurrent, nonradiative transitions are hardly covered in common textbooks, with the exception of the book by Birks, [112], which is out of print. We shall therefore give a more extensive treatment.

The rate for a nonradiative transition can be written as

$$k_{\mathrm{if}} = \frac{2\pi}{\hbar}|\langle\Psi_{\mathrm{el,f}}\Psi_{\mathrm{vib,f}}\Psi_{\mathrm{spin,f}}|\hat{H}'|\Psi_{\mathrm{el,i}}\Psi_{\mathrm{vib,i}}\Psi_{\mathrm{spin,i}}\rangle|^2\rho \quad (1.70)$$

where the perturbing Hamiltonian $\hat{H}'$ that induces the radiationless transition is the nuclear kinetic energy operator $\partial/\partial Q$. $Q$ is a normal mode displacement. When treating nonradiative transitions, one has to go beyond the Born–Oppenheimer approximation. Siebrand [111, 146] does this first by integrating over the electronic coordinates, thus writing Eq. (1.70) as

$$k_{\mathrm{if}} = \frac{2\pi}{\hbar}|\langle\Psi_{\mathrm{vib,f}}|\mathcal{J}|\Psi_{\mathrm{vib,i}}\rangle|^2\rho \text{ with}$$
$$\mathcal{J} = \langle\Psi_{\mathrm{el,f}}\Psi_{\mathrm{spin,f}}|\hat{H}'|\Psi_{\mathrm{el,i}}\Psi_{\mathrm{spin,i}}\rangle \quad (1.71)$$

and then inserting molecular wavefunctions and operators. In this way, he was able to separate Eq. (1.70) into the different components [111]. He arrives at the expression

$$k_{\mathrm{if}} = \frac{2\pi}{\hbar}\rho J^2 F \quad (1.72)$$

where $J$ contains the electronic coupling between the two states, while the overlap of the vibrational wavefunctions of the initial and final state is contained in the FC factor $F$. Formally, the rate equations for the radiative and nonradiative transitions, Eq. (1.6) and Eq. (1.72), are thus similar. We shall now discuss the factors $F$ and $J$.

#### 1.4.4.1 The Franck–Condon Factor *F* and the Energy Gap Law

The FC factor $F$ is given by the overlap of the overall vibrational wavefunction $|\langle\Psi_{\mathrm{vib,f}}|\Psi_{\mathrm{vib,i}}\rangle|^2$, where the initial state vibrational wavefunction has a vibrational energy of 0, $\Psi_{\mathrm{vib,i}} = \Psi_{\mathrm{vib,i}}(0)$, and the final state vibrational wavefunction has a vibrational energy E, $\Psi_{\mathrm{vib,f}} = \Psi_{\mathrm{vib,f}}(\mathrm{E})$. $\Delta E = (E - 0)$ is the energy gap between the 0–0 energies of the initial and final state. Siebrand, Robinson, and Frosch calculated how the FC factor changes with increasing energy difference $\Delta E$ [111, 128].

To describe the experimental results, it is sufficient to consider only one vibrational mode of the final state, that is the one with the highest frequency $\omega_{\mathrm{M}}$. Its vibrational quantum number $\upsilon_{\mathrm{M}}$ is given by $\upsilon_{\mathrm{M}} = \Delta E/\hbar\omega_{\mathrm{M}}$. The FC factors for the limiting cases of a displaced oscillators and a distorted oscillator are given in Box 1.11. For the general case of a displaced and distorted oscillator, evaluation of the FC factor results in an exponential dependence on $\Delta E/\hbar\omega$. As $J$ is constant with energy, this leads to an exponential dependence of the nonradiative transition rate on the energy difference between the initial and final state. This is well known as the *energy gap law* and is expressed as

$$k_{\mathrm{if}} \propto \exp\left(-\gamma\frac{\Delta E}{\hbar\omega_{\mathrm{M}}}\right) \quad (1.73)$$

with $\hbar\omega_{\mathrm{M}}$ being the vibrational quanta of the highest frequency mode, and $\gamma$ is a term that can be expressed through molecular parameters [111, 128, 129, 134]. The mode involved in the FC overlap is called an *accepting mode*. When several high-frequency modes are to be considered (Box 1.12), a correspondingly weighted term can be used though the limitation to the highest frequency mode is usually sufficient. Experimentally, the energy gap law has been well confirmed, both for organic aromatic hydrocarbons and for organometallic complexes and polymers (Figure 1.30).

#### 1.4.4.2 The Electronic Coupling *J*

$J$ contains the coupling between the initial and final electronic state. $J$ can be evaluated by first expanding the operator $\mathcal{J}$ in terms of normal mode displacements around the equilibrium position $Q_0$, $\mathcal{J} = \sum_{n=1}^{N}\frac{\partial\mathcal{J}}{\partial Q_n}(Q_n - Q_0)$. This is inserted into Eq. (1.71) and evaluated to yield Eq. (1.72).

**Box 1.12 Franck–Condon Factors Involving Several Modes**

A real molecule has not just one but several normal mode vibrations. This renders the expressions for the Franck–Condon factors a little more complicated [111]. When several normal modes $n$ with frequency $\omega_n$, vibrational quantum number $m_n$, and vibrational wavefunctions $\chi_n$ are involved, the overall vibrational wavefunction needs to be written as a product, $\Psi_{\mathrm{vib,f}}(\mathrm{E}) = \prod_{\mathrm{n}}\chi_n(m_n)$. Further, the transition may take place into any state $\Psi_{\mathrm{el,f}}\Psi_{\mathrm{vib,f}}\Psi_{\mathrm{spin,f}}$ with suitable total energy, implying that the general Franck–Condon factor in Eq. (1.25) becomes a sum $F = \sum_P P\left[\prod_{\substack{n=1\\ n\neq p}}^{N}|\langle\chi_{\mathrm{n,f}}(0)|\chi_{\mathrm{n,i}}(m_n)\rangle|\right]^2$. The operator $\sum_P P$ permutates the vibrational quanta $m_n$ among the N normal modes. This permutation is subject to the energy conservation condition $\sum m_n\hbar\omega_n = E$. In the end, the energy gap law is recovered. Due to the exponential dependence on the vibrational frequency, however, the use of a single highest-energy frequency is fully sufficient for most cases.

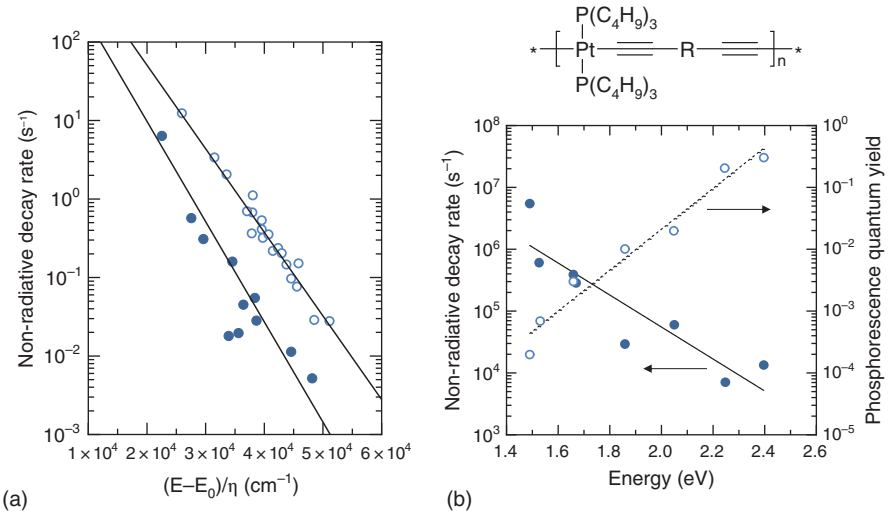


**Figure 1.30** The energy gap law. (a) Example for aromatic hydrocarbons: Dependence of the nonradiative decay rate $k_{nr}$ for a number of normal (open symbols) and deuterated (filled symbols) aromatic hydrocarbons on the normalized triplet energy $(E_T - E_0)/\eta$. $\eta$ is the relative fraction of hydrogen or deuterium atoms in the molecule. $E_0$ is a minor correction factor related to the Franck–Condon factor crossing for displaced and distorted oscillators, and it is $E_0 = 4000\ \mathrm{cm}^{-1}$ (0.5 eV) for protonated compounds and $E_0 = 5500\ \mathrm{cm}^{-1}$ (0.68) for deuterated compounds. Totally deuterated molecules included are (in order of decreasing $\tau$) benzene, triphenylene, acenaphthene, naphthalene, phenanthrene, crysene, biphenyl, p-terphenyl, pyrene, 1,2-benzanthracene, and anthracene. (After [147].) (b) Example for organometallic polymers: $k_{nr}$ and phosphorescence quantum yield as a function of the triplet state energy for a series of Pt-polymers with R = phenylene, alkoxy-substituted phenylene, thiophene, quinoline, bithiophene, quinoxaline, terthiophene, and benzothiadiazole (in order of decreasing $T_1$ energy). The lines indicate exponential fits. (Data from Ref. [148].)

In this process, Siebrand assumes that a single oscillator $p$ accounts for most of the induced transition probability, and that this oscillator is only slightly perturbed by the transition [111, 146]. With this, he arrives at

$$J = \frac{\partial \mathcal{J}}{\partial Q_p} \frac{\hbar\omega_p}{2k_p} \langle \chi_{p,f}(0) | \chi_{p,i}(0) \rangle \tag{1.74}$$

where $\hbar\omega_p$ is the vibrational quantum of the mode that induces the transition, and $k_p$ is its force constant. The mode associated with $J$ is called a *promoting mode* for the transition.

The electronic coupling contains the electronic and spin wavefunctions (see Eq. (1.71)), implying that for spin, symmetry, and parity considerations, the same selection rules as for the corresponding radiative transitions apply. Internal conversion between states of the same parity may occur nevertheless since the radiationless transition occurs into a higher vibronic level of the final state that may differ in symmetry and parity from the zero-point level of the final state [112].

Regarding the spin, Eq. (1.71) implies that spin-orbit coupling is required for intersystem crossing to occur. A large spin-orbit coupling thus allows for a large intersystem crossing rate. This agrees with experimental observations on the intersystem crossing rate. For example, the $S_1 \rightarrow T_1$ transition rate can be measured directly when an $S_1$ state is created by an excitation pulse, and then the time is measured for a $T_n \leftarrow T_1$ absorption signal to appear. Such measurements are referred to as pump-probe experiment, transient absorption measurement, or flash photolysis spectroscopy. Typical intersystem crossing rates for $S_1 \rightarrow T_1$ are $k_{ISC} \approx 10^{12}\mathrm{s}^{-1}$ for organometallic complexes and $k_{ISC} \approx 10^6\mathrm{s}^{-1} - 10^9\mathrm{s}^{-1}$ for organic oligomers (see also Table 1.4) [120]. Intersystem crossing rates into higher triplet states are often faster due to the smaller energy gap. For example, for terthiophene, the dominant intersystem crossing channels from $S_1$ are the exothermic $S_1 \rightarrow T_3$ pathway and the endothermic $T_4 \leftarrow S_1$ pathway, while the $S_1 \rightarrow T_1$ route is negligible [120]. Intersystem crossing rates for the $T_1 \rightarrow S_0$ transition depend exponentially on the $T_1$ energy and are in the range of $0.1\text{–}10\ \mathrm{s}^{-1}$ for aromatic hydrocarbons [112, 116] and $10^3\text{–}10^6\ \mathrm{s}^{-1}$ for organometallic compounds (see Figure 1.30) [148]. This compares against the corresponding radiative rates of 0.1 and $10^3\ \mathrm{s}^{-1}$, respectively.

#### 1.4.4.3 Accepting Modes, Promoting Modes, and the Isotope Rule

From Eq. (1.72), it is evident that both accepting and promoting modes play a role in the nonradiative transition. While the significance of the accepting modes was evident early on, the contribution of the promoting mode has only become apparent in the course of time, in particular through work on organometallic complexes and rare earth complexes [144, 145].

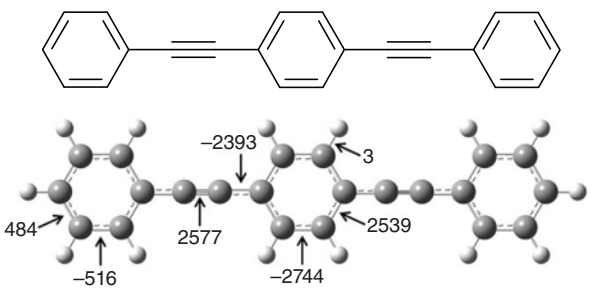


**Figure 1.31** The geometry of a phenylene–ethynylene model trimer. The changes in bond length from the geometry of the ground state $S_0$ to excited state $T_1$ are indicated for selected bonds in $10^{-15}$ m.

It may be helpful to associate some intuitive picture with these modes. To illustrate this, consider the $T_1 \rightarrow S_0$ transition in the molecule shown in Figure 1.31. Normal modes of high frequency in this molecule include the stretching vibration of the C—H bond on the benzene ring, the stretching vibration of the C—C triple bond, and a breathing mode of the benzene ring. As detailed in Box 1.8, the associated vibrational quanta for these modes are $3000\,\mathrm{cm}^{-1}$ (378 meV), $2100\,\mathrm{cm}^{-1}$ (260 meV), and $1600\,\mathrm{cm}^{-1}$ (198 meV), respectively. Next consider the equilibrium geometries in the $T_1$ state and in the $S_0$ state. The changes in bond lengths between $S_0$ and $T_1$ are indicated in Figure 1.28 for the model trimer phenylene ethynylene. Evidently, changing the electronic state from $T_1$ to $S_0$ is associated with changes in the carbon–carbon bond lengths in the benzene ring and along the molecular axis in the range of 2–3 pm. In contrast, the carbon–hydrogen bond length changes by 3 fm, i.e. it remains largely unaffected by the electronic transition. Therefore, the electronic transition can couple to the C–C triple bond stretching vibration and to the benzene ring breathing mode, as is evident in the vibrational structure of the phosphorescence spectra. The converse also applies – these vibrations can act as promoting modes to the isoenergetic nonradiative transition from $T_1$ into $S_0$. The electronic energy associated with $T_1$ now needs to be accepted by an overtone of a vibration in $S_0$, the accepting mode, which will then dissipate it to the environment. For this transfer of energy to be efficient, the FC factor should be large, implying that the accepting mode should have a high frequency (c.f. Eq. (1.73)). In the case of the phenylene ethynylene model molecule shown in Figure 1.28 as well as for the Pt polymer shown in Figure 1.30 with R=phenylene [103], the highest energy mode is the C–H stretching mode. However, the C–H mode does not couple to the electronic $T_1 \rightarrow S_0$ transition, as evidenced by its negligible displacement. This is understandable since it oscillates nearly orthogonal to the direction of both the changes in the nuclei positions and the changes in the electron density that accompany the electronic $T_1 \rightarrow S_0$ transition. So, despite its high frequency, the C–H mode does not act as an accepting mode. The C–C triple bond stretch, in contrast, couples well and has a high vibrational frequency that makes it suitable as an accepting mode. In this example, the C–C triple bond stretching vibration acts as both a promoting mode and an accepting mode. In the general case, they can differ.

The well-established way to investigate whether a mode controls the nonradiative decay as an accepting mode is to replace an atom involved by an isotope of different mass. The vibrational frequency of a mode depends on the effective mass $\mu$ of the atoms involved and the force constant $k$ by $\omega = \sqrt{k/\mu}$. For the simple case of a stretching vibration between two atoms with masses $m_1$ and $m_2$, $\mu = m_1 m_2/(m_1 + m_2)$. Replacing one of them with a heavier atom increases the effective mass and reduces the vibrational frequency. This, in turn, decreases the nonradiative transition rate according to Eq. (1.73). A classic example for this is the replacement of hydrogen by deuterium in aromatic hydrocarbons such as polyacenes. This reduces the frequency of the C–H vibration from about $3000\,\mathrm{cm}^{-1}$ to about $2200\,\mathrm{cm}^{-1}$ and leads to a concomitant observed reduction in the nonradiative decay rate (Figure 1.30).

#### 1.4.4.4 Implications of the Energy Gap Law

The energy gap law (Eq. (1.73)) has a number of consequences. One of it is that internal conversion from $S_2 \rightarrow S_1$ or from $T_2 \rightarrow T_1$ is usually fast ($\sim 10^{12}$ s$^{-1}$) compared to the radiative decay rate of $S_2 \rightarrow S_0$ ($\sim 10^9$ s$^{-1}$) or $T_2 \rightarrow S_0$, as the $S_2$–$S_1$ and $T_2$–$T_1$ energy gaps are small. As a result, emission always occurs from the lowest excited state of a spin manifold. This is empirically known as *Kasha's rule*. This no longer applies when the $S_2$–$S_1$ energy difference becomes large, such as in excess of 1 eV, and emission from $S_2$ can be observed. As this was first observed for Azulene and later also for its derivatives, this phenomenon is referred to as *Azulene anomaly* [112, 149–152].

Another implication of the energy gap law is that an endothermic transition to an energetically close state may provide a faster nonradiative decay channel than an exothermic transition to a state that is at much lower energy. The temperature dependence of the nonradiative transition rate is empirically frequently found to take a form of

$$k_{\mathrm{nr}}(T) = k_{\mathrm{nr}}^0 + k'_{\mathrm{nr}} \exp\left(-\frac{E_{\mathrm{a}}}{kT}\right) \tag{1.75}$$

with $k_{\mathrm{nr}}^0$ and $k'_{\mathrm{nr}}$ being independent of temperature and $E_{\mathrm{a}}$ being an activation energy.

Finally, the energy gap law is also the reason why nonradiative decay rate seriously competes with the radiative rate for the $T_1 \rightarrow S_0$ transition – note that intersystem crossing is required in both cases – while for the $S_1 \rightarrow S_0$ transition, internal conversion to the ground state is negligible

compared to the radiative decay. Common $T_1$ energies are in the range of 1–2 eV, while $S_1$ energies often range from 2 to 3 eV.

#### 1.4.4.5 The Strong Coupling Limit

In general, theory distinguishes between the two limiting cases of weak coupling and strong coupling illustrated in Figure 1.32. The above considerations and equations in Sections 1.4.4.1–1.4.4.4 apply to the weak coupling limit. This is the case when the potential energy surfaces of the initial and final state are only weakly displaced so that the surfaces only intersect far away from the minimum of the upper state surface. For aromatic hydrocarbons, this is considered to be fulfilled [134].

Strong coupling applies when the minima of the potential energy curves of the initial and final state are strongly displaced so that the potential curves intersect near to the potential minimum of the higher energy state. This case has been considered for some metal complexes, where the metal–ligand bond length can change significantly for a transition between two states [145]. The geometric reorganization energy $E_{\mathrm{rel}} = \sum_j S_j \hbar\omega_j$ is taken as a quantitative criterion to distinguish the two limits. If it is smaller than the mean vibrational energy $\hbar\langle\omega\rangle = \sum_j \hbar\omega_j/N$ of the molecule, the weak coupling limit is fulfilled. Mathematically, $E_{\mathrm{rel}} \lesssim \hbar\langle\omega\rangle$ implies the weak coupling limit and $E_{\mathrm{rel}} \gg \hbar\langle\omega\rangle \tanh\left(\frac{\hbar\langle\omega\rangle}{2kT}\right)$ identifes the strong coupling limit [134]. A more practical equivalent condition is $\sum_j S_j \lesssim 1$ for the weak coupling limit and $\sum_j S_j \gg 2$ for the strong coupling limit.

In the strong coupling limit, the nonradiative transition rate becomes

$$k_{\mathrm{nr}} \propto \frac{1}{\sqrt{E_{\mathrm{rel}}}} \exp\left(-\frac{2E_{\mathrm{A}}}{\hbar\langle\omega\rangle}\right), E_{\mathrm{A}} = \frac{(\Delta E - E_{\mathrm{rel}})^2}{4E_{\mathrm{rel}}} \qquad (1.76)$$

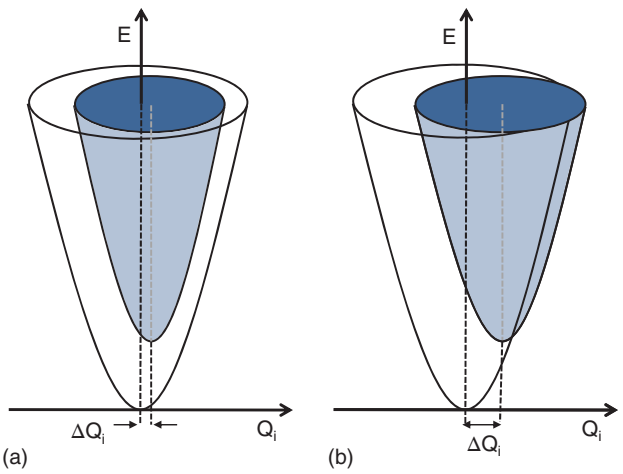


**Figure 1.32** The potential energy curves (a) for the case of weak coupling and (b) for the case of strong coupling between the two states. (After [134].)

where $\Delta E$ is the energy gap between the two states. Eq. (1.71) applies at "low" temperature, i.e. $\hbar\langle\omega\rangle \gg kT$, which is usually fulfilled. Compared to the weak coupling case, there are two major differences. First, the dependence on the energy gap is not exponential but Gaussian. Second, the rate is not controlled by the highest energy vibrational mode but by an effective mode of mean energy. Essentially, all vibrations can act equally as accepting modes. As a result, replacing an atom with an isotope has little effect on the transition rate. In the unlikely situation of the molecule being immersed in a heat bath such that $\hbar\langle\omega\rangle \ll kT$, the functionality obtained is

$$k_{\mathrm{nr}} \propto \frac{1}{\sqrt{E_{\mathrm{rel}}}} exp\left(-\frac{E_{\mathrm{A}}}{kT}\right) \qquad (1.77)$$

One may notice the formal similarity to the Marcus equation of charge transfer [153]. When Englman comes to this equation after an about 10-page-long derivation in his original paper, he succinctly comments "This equation has a general appearance of a conventional rate equation, where the energy $E_{\mathrm{A}}$ plays the role of the activation energy as might have been guessed by the intelligent chemist on intuitive grounds" [134].

The questions on which coupling limit applies, and on the role of accepting modes and promoting modes in the weak coupling limit, have been addressed in particular for metal, organometallic, and rare earth complexes [145]. In these materials, the nonradiative decay can be very competitive with the radiative decay channel. The nonradiative decay can be reduced by replacing the atom involved in the vibrations with heavier ones, e.g. replacing C–H with C–D. This method is only applicable if the nonradiative decay is controlled by a high-frequency accepting mode in the weak coupling regime. In the strong coupling limit, this does not work.

### 1.4.5 Basic Photophysical Parameters: Lifetimes and Quantum Yields

Those interested in organic semiconductor devices may ask, quite justifiably, why they should care about the origins of radiative or nonradiative transition rates. The answer is that the radiative and nonradiative decay rates control the lifetime $\tau$ of an excited state, the quantum yield of emission from an excited state, and the quantum yield of transitions between states. In this way, $k_{\mathrm{r}}$ and $k_{\mathrm{nr}}$ determine whether an organic semiconductor material is suitable for application in a LED or solar cell. This is illustrated in Figure 1.33. By definition, the radiative decay rate $k_{\mathrm{r}}$ gives the number of radiative decays per second, and a nonradiative decay rate $k_{\mathrm{nr}}$ corresponds to the number of nonradiative decays per second. Since their sum is the total number of decays per second, the inverse of it defines the lifetime of an excited state, also called the *natural lifetime*.

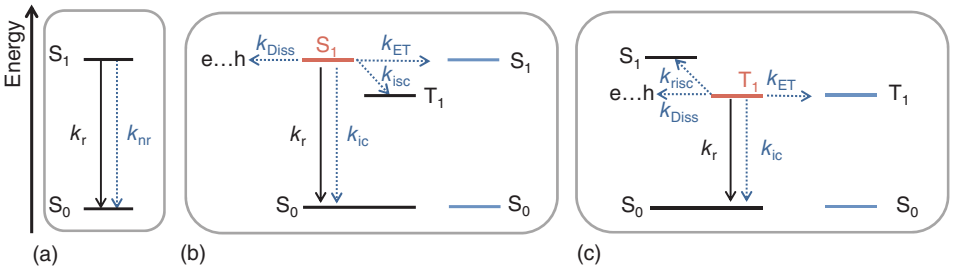


**Figure 1.33** State diagram (a) indicating the radiative and nonradiative decay from $S_1$ to $S_0$ with rates $k_r$ and $k_{nr}$ in a general fashion. Several possible nonradiative decay routes are indicated (b) from $S_1$ and (c) from $T_1$, such as internal conversion ($k_{IC}$), intersystem crossing ($k_{ISC}$) (for $S_1$) or reverse intersystem crossing ($k_{RISC}$) (for $T_1$), energy transfer ($k_{ET}$), and exciton dissociation ($k_{diss}$).

$$\tau = \frac{1}{k_r + k_{nr}} \tag{1.78}$$

This is the experimentally measured lifetime that appears as the decay constant in the mono-exponential intensity decay of the luminescence intensity of a state, $I(t) = I_0 e^{-t/\tau}$. This is a consequence of the fact that the luminescence intensity is equal to the concentration of excitations that decay per second, $I(t) = k_r n(t)$, with $n(t) = n_0 e^{-t/\tau}$ denoting the time-dependent concentration of excitations. In rate equations, it is also customary to use a square bracket to indicate a concentration of, e.g. singlet or triplet excitations, such as $[S_1]$ or $[T_1]$. One may also define a *radiative lifetime* $\tau_0 = 1/k_r$ that gives the theoretical maximum lifetime the excited state may have assuming no nonradiative decay channels present.

There is usually only one significant radiative pathway that contributes to $k_r$. For an $S_1$ state, that is the $S_1 \rightarrow S_0$ transition. In contrast, several processes with individual rates $k_{nr_i}$ add to the overall nonradiative decay rate $k_{nr} = \sum_i k_{nr_i}$. When considering an individual molecule, the nonradiative decay processes that can occur are the fundamental ones discussed in Section 1.4.4, i.e. internal conversion with a rate $k_{IC}$ and intersystem crossing with a rate $k_{ISC}$. In a condensed phase such as a solution or a film, an excited state may further dissociate into free carriers with a rate $k_{diss}$ or transfer its energy to another state with $k_{ET}$. The mechanisms for dissociation and energy transfer are discussed in Chapter 3. A general expression for the lifetime of an excited state of a molecule in the gas phase is thus

$$\tau = \frac{1}{k_r + \sum_i k_{nr_i}}, \tag{1.79}$$

which may include contributions such as

$$\tau = \frac{1}{k_r + k_{IC} + k_{ISC} + k_{diss} + k_{ET}}, \tag{1.80a}$$

For the $S_1$ state and

$$\tau = \frac{1}{k_r + k_{IC} + k_{RISC} + k_{diss} + k_{ET}}, \tag{1.80b}$$

For the $T_1$ state, as illustrated in Figure 1.33. Evidently, rates that are more than two orders of magnitude lower than others do not need to be considered in practice. For example, for the singlet excited state of an individual molecule, the internal conversion rate is insignificant due to the usually large gap between $S_1$ and $S_0$, thus $\tau_{S1} = (k_{Fl} + k_{ISC})^{-1}$, while $\tau_{T1} = (k_{Ph} + k_{IC,T1})^{-1}$ includes the dominant contributions for the triplet state of the same molecule, unless the energy gap between $S_1$ and $T_1$, $\Delta E_{ST}$, becomes small ($\Delta E_{ST} < 0.3$ eV) so that $\tau_{T1} = (k_{Ph} + k_{RISC} + k_{IC,T1})^{-1}$.

The ratio of the radiative decay rate to the total decay rate of an excited state defines its photoluminescence efficiency. Since it measures the fraction of photon quanta that decay radiatively per unit time, it is also referred to as photoluminescence quantum yield $\Phi_{PL}$. If every photon absorbed creates an excited state from which the radiative decay takes place, the PL quantum yield thus becomes

$$\Phi_{PL} = \frac{k_r}{k_r + \sum_i k_{nr_i}} = \tau k_r = \frac{\tau}{\tau_0} \tag{1.81}$$

Accordingly, the quantum yield for the fluorescence of a molecule in the gas phase is given by $\Phi_{Fl} = k_{Fl}/(k_{Fl} + k_{ISC}) = k_{Fl}\tau_{S1}$ (assuming that internal conversion is insignificant). For the phosphorescence yield, the generation efficiency of the triplet excited state needs to be taken into account. The $T_1$ state is formed by intersystem crossing with a quantum yield

$$\Phi_{ISC} = \frac{k_{ISC}}{k_{ISC} + k_{Fl} + k_{nr,S1}} \tag{1.82}$$

The ratio between the photon quanta emitted from the triplet state to the absorbed photon quanta is therefore

$$\Phi_{Ph} = \Phi_{ISC} \cdot \frac{k_{Ph}}{k_{Ph} + \sum_i k_{nr_i}} = \Phi_{ISC} \cdot \frac{k_{Ph}}{k_{Ph} + k_{RISC} + k_{IC,T1}} = \Phi_{ISC} k_{Ph} \tau_{T1} \tag{1.83}$$

A particular case is that of a molecule where the singlet $S_1$ state is populated not only by absorption but also by thermally activated reverse intersystem crossing, as shown in

Figure 1.33c. In addition to the usual, *prompt fluorescence (PF)* from $S_1$ that is dominated by its radiative decay rate $k_r$, one also observes, with lower intensity, a fluorescence at later times after the optical excitation pulse. This *delayed fluorescence (DF)* occurs when an $S_1$ state first converts to a $T_1$ state (with rate $k_{ISC}$), and then transfers back by thermally activated reverse intersystem crossing (with rate $k_{RISC}$) to $S_1$, from where it finally decays radiatively. This phenomenon of *thermally activated delayed fluorescence (TADF)* is discussed further in Sections 3.5.3 and 4.2.4. The associated photophysics is intricate and has been thoroughly described by Berberan-Santos *et al.* [154].

The PL quantum yield of a TADF emitter, accounting for the recycling of singlet and triplet states, is described by Eq. (1.84)

$$\Phi_{PL} = \Phi_{PF} + \Phi_{DF} = \sum_{i=0}^{\bar{n}} \Phi_{PF}(\Phi_{ISC}\Phi_{RISC})^i = \Phi_{PF}\frac{1}{1-\Phi_{ISC}\Phi_{RISC}} \quad (1.84)$$

$\Phi_{PF}$, $\Phi_{DF}$, $\Phi_{ISC}$, and $\Phi_{RISC}$ in Eq. (1.84) denote the quantum yields of prompt fluorescence, delayed fluorescence, intersystem crossing, and reverse intersystem crossing, respectively, and $\bar{n}$ is the number of $S_1 \rightarrow T_1 \rightarrow S_1$ cycles prior to $S_1 \rightarrow S_0$ radiative decay, as depicted in Figure 1.33. The quantum yield of prompt fluorescence, $\Phi_{PF} = k_{Fl}/(k_{Fl} + k_{ISC}) = k_{Fl}\tau_{S1}$ (assuming that internal conversion is insignificant), and the quantum yield of intersystem crossing ($\Phi_{ISC}$), are defined by Eq. (1.82). Reverse intersystem has a quantum yield given by

$$\Phi_{RISC} = \frac{k_{RISC}}{k_{RISC} + k_{Ph} + k_{IC,T1}} \quad (1.85)$$

Evidently, for a strong yield of singlet formation by RISC (i.e. $\Phi_{RISC} \approx 1$), it is necessary that $k_{RISC} \gg k_{Ph} + k_{IC,T1}$. This condition can be met when using fluorescent molecules with a minimal energy gap between the lowest singlet and triplet states ($\Delta E_{ST}$). As discussed in Section 1.3.4, the exchange energy between states dominated by $\pi\pi^*$ transitions is typically 0.7–1.0 eV, meaning that $\Delta E_{ST}$ is much greater than the thermal energy at room temperature, and hence the reverse intersystem crossing rate ($k_{RISC}$) is small. The crucial aspect in designing molecules with reduced exchange energy is minimizing the overlap between the HOMO and LUMO orbitals by spatially separating these frontier orbitals so that the excited states are associated with charge-transfer transitions. Simultaneously, it is important to maintain the molecular structure sufficiently rigid to keep the $T_1 \rightarrow S_0$ internal conversion rate ($k_{IC,T1}$) low. Metal-free purely organic TADF emitters are employed in the development of high-efficiency OLEDs, as discussed in Section 4.2.4.

**Table 1.1** Experimentally measured fluorescence lifetimes.

| Position | Compound | $\tau_{S1}$ in nanoseconds | Reference |
|---|---|---|---|
| 1 | MeLPPP | 0.30 | [155] |
| 2 | MEH-PPV in toluene solution at 295 K | 0.45 | [43] |
| | MEH-PPV in $CHCl_3$ solution at 295 K | 0.35 | [156] |
| 3 | PFO | 0.43 | [44] |
| 4 | OPV3, OPV4, OPV5, OPV6, and OPV7 in $CHCl_3$ solution at 295 K | 1.70, 1.32, 0.73, 0.52, 0.45 | [157] |
| 5 | PF-trimer, -pentamer, and -heptamer in thin film at 295 K | 0.67, 0.58, 0.52 | [105] |
| 6 | Biphenyl, *p*-terphenyl, and *p*-quaterphenyl in cyclohexane at 295 | 16, 1.0, 0.8 | [112] |
| 7 | Fluorene in cyclohexane at 295 K | 10 | [112] |
| 8 | Benzene naphthalene, anthracene, and tetracene in cyclohexane at 295 K | 30, 100, 5, 6 | [112] |
| 9 | Pyrene in cyclohexane at 295 K | 450 | [112] |
| 10 | Perylene in cyclohexane at 295 K | 6 | [112] |

It is useful to have some idea about the magnitudes of different photophysical parameters. Tables 1.1–1.4 provide a compilation of a few selected data for a basic orientation. More extensive information can be found in the books by Birks, Pope&Swenberg, and Turro for the class of organic molecules, in the book by Yersin for organometallic complexes and, for the polymers and oligomers, in the original papers quoted in the tables [21, 86, 112, 116].

From the tables, it is evident that the fluorescence lifetime of polymers tends to be below 1 ns. As the radiative rate for a fully allowed transition is at most $10^9\ s^{-1}$, the short lifetime in polymers reflects a comparable nonradiative decay rate. The reduction in lifetime with oligomer length observed for the oligomers can be attributed to both an increase in the oscillator strength of the transition, evident from the increase in extinction coefficient, and an increase in nonradiative decay [157]. The low oscillator strength for the $S_1 \leftarrow S_0$ transitions for benzene, naphthalene, and pyrene is due to the fact that this transition is partially forbidden by symmetry selection rules. The "obvious" transition seen in the absorption spectra is therefore the allowed $S_2 \leftarrow S_0$ transition. For longer polyacenes, the

**Table 1.2** Fluorescence quantum yields and extinction (Eq. (1.10)) or absorption (Eq. (1.8)) coefficients. Extinction coefficients are given at the peak of the $S_1 \leftarrow S_0$ transition unless stated otherwise.

| Position | Compound | $\Phi_{Fl}$ | $\varepsilon$ in $mol^{-1}\ cm^{-1}$ | Reference |
|---|---|---|---|---|
| 1 | PFO as (glassy phase) thin film, nematic glass, or crystal, all at 20 K | 0.8–0.9 | – | [44] |
| | PFO in the β-phase at 20 K | 0.42 | | [44] |
| | PFO as amorphous thin film or β-phase at 295 K | 0.53, 0.55 | | [44] |
| | PFO as crystal or nematic glass at 295 K | 0.65, 0.80 | | [44] |
| | PF0 as glassy phase thin film | | Here, α is given instead: $\alpha = 250\,000\ cm^{-1}$ | [106] |
| 2 | PPV as thin film at 10 K, at 295 K | 0.40, 0.08 | | [158] |
| | MEH-PPV in $CHCl_3$ solution at 295 K | 0.35 | | [156] |
| 3 | OPV3 in $CHCl_3$ solution at 295 | 0.62 | 44 000 | [157] |
| | OPV4 in $CHCl_3$ solution at 295 | 0.76 | 68 000 | |
| | OPV5 in $CHCl_3$ solution at 295 | 0.49 | 88 000 | |
| | OPV6 in $CHCl_3$ solution at 295 | 0.41 | 107 000 | |
| | OPV7 in $CHCl_3$ solution at 295 | 0.25 | 142 000 | |
| 4 | PF-trimer | 0.41 | 85 100 | [105] |
| | PF-pentamer | 0.42 | 135 900 | |
| | PF-heptamer | 0.44 | 196 800 | |
| | | all in thin film at 295 K | all in chlorobenzene solution at 295 K | |
| 5 | Biphenyl | 0.15 | 17 000 for $S_2$ at 5.0 eV ($S_1$ not observed), in light petroleum | [112] |
| | *p*-terphenyl | 0.77 | 33 100 for $S_1$ at 4.46 eV in heptane | |
| | *p*-quaterphenyl | 0.74 | 36 300 for $S_1$ at 4.28 eV in heptane | |
| | | all in cyclohexane at 295 | | |
| 6 | Fluorene | 0.66 in cyclohexane at 295 K | 10 000 for $S_1$ in heptane | [112] |
| 7 | Benzene | 0.06 | 250 for $S_1$ at 4.87 eV, | [112] |
| | | | 8800 for $S_2$ at 6.08 eV, | |
| | Naphthalene | 0.19 | 270 for $S_1$ at 4.12 eV, 5600 for $S_2$ at 4.51, | |
| | Anthracene | 0.30 | 8500 for $S_1$ at 3.31 eV, | |
| | Tetracene | 0.17 | 14 000 at 2.63 eV | |
| | all absorptions in heptane, all emissions in cyclohexane at 295 K | | | |
| 8 | Pyrene | 0.65 in cyclohexane at 295 K | 510 for $S_1$ at 3.53 eV, | [112] |
| | | | 55 000 for $S_2$ at 3.70 eV, in light petroleum | |
| 9 | Perylene in cyclohexane at 295 K | 0.89 | 39 500 for $S_1$ at 2.85 eV | [112] |

**Table 1.3** Experimentally measured phosphorescence lifetimes.

| Position | Compound | $\tau_{T1}$ | Reference |
|---|---|---|---|
| 1 | MeLPPP in mixed toluene:MTHF solution at 77 K | 1.0 s | [159] |
| | MeLPPP in film at 10 K and at 295 K | 0.5 s and $10^{-4}$ s | [160] |
| 2 | MEH-PPV in film, both at 5 K and 295 K | 50 µs | [161] |
| | OPV2, OPV3, OPV4, OPV5, OPV6, and OPV7 in MTHF at 80 K | 7.9 ms, 3.6 ms, 3.4 ms, 3.7 ms, 2.9 ms | [157] |
| 3 | FIrpic in CDBP matrix at 295 K | 1.4 µs | [162] |
| 4 | Ir(ppy)3 in solution at 295 and at 2 K | 2.6 µs, 140 µs | [86] |
| 5 | Pt-polymers in thin films at 20 K with $T_1$ from 2.5 eV to 1.5 eV | 100 µs to 0.1 µs | [148] |

**Table 1.4** Illustration of the heavy atom effect on naphthalene [112].

| Compound | $\Phi_{Fl}$ | $k_{Fl}$ | $k_{ISC}$ |
|---|---|---|---|
| Naphthalene | ~0.2 | $\sim 10^6$ | $5 \times 10^6$ |
| 1-Chloronaphthalene | ~0.05 | $\sim 10^6$ | $5 \times 10^8$ |
| 1-Bromonaphthalene | ~0.002 | $\sim 10^6$ | $\sim 10^9$ |
| 1-Iodonaphthalene | ~0.000 | $\sim 10^6$ | $\sim 10^{10}$ |

energy of the allowed transition decreases below that of the symmetry-forbidden transition, thus resulting in an intense $S_1 \leftarrow S_0$ signal. Fluorescence quantum yields for polymers vary and depend on sample morphology and also on purity. In contrast, quantum yields for molecules or oligomers are more uniform. Phosphorescence lifetimes for organic compounds are in the range of milliseconds to seconds, unless the $T_1$ state is very low as for MEH-PPV. The phosphorescence lifetimes in organometallic compounds are in the µs regime and depend on the triplet state energy, according to the energy gap law.

## 1.5 Spectroscopic Methods

Photophysical parameters such as the fluorescence and phosphorescence lifetimes and quantum yields, as well as their spectra, are usually measured in a film or in solution. The solution may be liquid (at room temperature), frozen (for temperatures below room temperature), or solid (i.e. frozen at room temperature). Typical organic solvents employed for a *liquid solution* include toluene, xylene, tetrahydrofuran (THF), chloroform ($CHCl_3$), dichloromethane ($CH_2Cl_2$), and many others. Good solubility of a material is obtained when the solubility parameter of the solvent and the material to be dissolved, the solute, are similar (see Box 1.13). While chlorinated solvents such as chloroform and dichloromethane are popular since they dissolve many semiconducting polymers particularly well, one should keep in mind that they are more harmful than most nonchlorinated solvents and the solutions are chemically less stable.

A *frozen solution* may become crystalline or form a glass, depending on the solvent. The term *solid solution* refers to the situation where a small amount of the molecule of interest, such as a chromophore or polymer, is dissolved in an electronically inert material, the matrix. Typical matrix materials are polystyrene (PS) and polymethoxymethacrylate (PMMA), also known as plexiglass. Both are transparent in the visible spectral range and electrically insulating. Thin films of a solid solution can be prepared by spin-coating. This is done by mixing the two materials, adding an organic solvent, putting a droplet of the liquid onto a rotating substrate, and waiting for the organic solvent to evaporate.

For spectroscopic investigations, thin films of neat material, blends, or solid solutions may be prepared on transparent substrates by a variety of techniques such as spin-coating, dip-coating, or blade-coating. Dip-coating consists essentially in dipping the substrate into the solution of material and retracting it, while blade-coating implies distributing the solvent over the substrate with a horizontal, steadily moved blade. The preferred substrate is the quartz-glass spectrosil B which is transparent far into the UV. Be aware that even apparently transparent substrates may have a weak absorption or emission feature that is worth checking for when observing a weak unexpected feature in a spectrum.

### 1.5.1 Photoluminescence Spectra, Lifetimes, and Quantum Yields

Any luminescence measurement consists of the same generic setup shown in Figure 1.34. Light from an excitation source is directed onto the sample using suitable optics. The light emitted from the sample is collected, again by suitable optics, and recorded by a detector. If one is interested in the spectrum, the emitted light needs to be dispersed in some way, for example, by placing a monochromator or spectrograph in front of the detector. The signal recorded by the detector needs to be corrected for the spectral response of the measurement unit,

**Box 1.13 Hildebrand and Hansen Solubility Parameters**

The character of a solvent can be parameterized in terms of the Hildebrand solubility parameter δ [163]. It gives a measure for the attractive strength between molecules of a material and corresponds to the square root of the cohesive energy density, $\Delta E$.

$$\delta = \sqrt{\frac{\Delta E}{V}} \tag{B1.13.1}$$

with V being the volume. The enthalpy of mixing, $\Delta H$, between the polymer and the solvent depends on the difference in the solubility parameters of the polymer and solvent according to

$$\frac{\Delta H}{V} = (\delta_{\text{polymer}} - \delta_{\text{solvent}})^2 \Phi_{\text{polymer}} \Phi_{\text{solvent}} \tag{B1.13.2}$$

where $V$ is the volume of the mixture and $\Phi$ is the volume fraction. Consequently, good mixing is observed when polymer and solvent have the same $\delta$. A few illustrative values are listed below for selected solvents and polymers. For many compounds, values of $\delta$ are quoted in common handbooks or in the technical report by the International Union of Pure and Applied Chemistry (IUPAC) [164]. which also contains the refractive indices and dielectric constants of many solvents. Be aware that $\delta$ may either be given in the popular units of $\sqrt{\text{cal/cm}^3}$ or in SI units $\text{MPa}^{1/2}$, with 2.046 $\delta$ ($\text{MPa}^{1/2}$) = 1 $\delta$ ($\text{cal}^{1/2}\text{cm}^{-3/2}$), see Table B1.13.1.

There are also other solubility parameters available that use different definitions, with the most widely known being the Hansen solubility parameter. The key idea of Hansen was to explicitly separate the different contributions to the cohesive energy density into contributions arising from dispersion (London) forces, $\Delta E_{\text{d}}$, polar forces, $\Delta E_{\text{p}}$, and hydrogen bonding, $\Delta E_{\text{h}}$ [169]. Hence, from

$$\Delta E = \Delta \text{E}_{\text{d}} + \Delta E_{\text{p}} + \Delta E_{\text{h}} \tag{B1.13.3}$$

**Table B1.13.1** List of Hildebrand solubility parameters.

| Compound | $\text{cal}^{1/2}\text{cm}^{-3/2}$ | $\text{MPa}^{1/2}$ |
|---|---|---|
| n-hexane [164] | 7.3 | 14.9 |
| m-xylene, p-xylene [164] | 8.8 | 18.0 |
| Toluene [164] | 8.9 | 18.2 |
| o-xylene [164] | 9.0 | 18.4 |
| Ethyl acetate[164] | 9.0 | 18.4 |
| Chloroform [164] | 9.2 | 18.9 |
| Tetrahydrofuran [164] | 9.3 | 19.0 |
| Acetone [164] | 9.6 | 19.7 |
| Dichloromethane [164] | 9.9 | 20.3 |
| Cyclopentanone [164] | 10.4 | 21.3 |
| Acetonitrile [164] | 11.8 | 24.2 |
| Polystyrene [165] | 9.1 | 18.7 |
| Poly(methyl methacrylate), PMMA [165] | 9.3 | 19.0 |
| PFO [166] | 9.1 – 9.3 | |
| MEH-PPV [167, 168] | 8.9 – 9.4 | |
| P3HT [163] | 9.3 | |

By using (B1.13.1), it is straightforward to arrive at

$$\delta^2 = \delta_{\text{d}}{}^2 + \delta_{\text{p}}{}^2 + \delta_{\text{h}}{}^2 \tag{B1.13.4}$$

Note that the solubility parameter of a given solvent is considered as a vector with components $\delta_{\text{d}}$, $\delta_{\text{p}}$, and $\delta_{\text{h}}$, along a dispersion axis, a polar axis, and a hydrogen bonding axis, respectively. For the Hildebrand solubility parameter, a compound is well soluble in a solvent when the difference between their values is small. In contrast, for the Hansen solubility parameter, their vectorial distance needs to be small. Values for the Hansen solubility parameters can be found in Ref. [169].

i.e. the spectral response of the excitation source, the optical pathway of the light, and the spectral response of the detector. This is usually done by taking a reference measurement with illumination yet without sample and dividing by it. Frequently, this step is already included in the software of the detection unit (provided it was calibrated after incorporation into the experimental setup).

If one is interested in the lifetime of the emitting state, a light pulse is used to excite the sample and the emitted light intensity is recorded as a function of time. Correction for the temporal response of the detection unit is only required when the decay time of the signal comes close to the temporal response of the detection unit.

The different measurement techniques only differ by the choice of excitation source and detection unit. These choices are dictated by the excitation mode needed (continuous or pulsed) and the time scale desired for the detection. Concerning the optics, a combination of lenses may be used or, alternatively, a glass fiber bundle. While combining lenses requires a little knowledge about the laws of optics, glass fiber bundles are very easy to use.

#### 1.5.1.1 Steady-State Spectra and Quantum Yields

A simple way to measure the time-integrated luminescence spectrum is to place the sample in a fluorescence spectrometer and to press the "run" button. In these machines, light from a xenon lamp or a deuterium lamp is directed

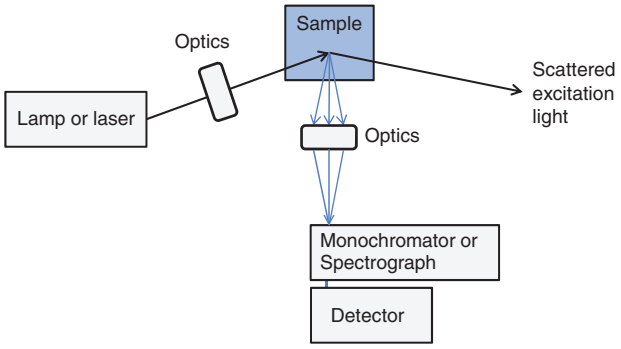


**Figure 1.34** Generic setup for measuring photoluminescence. The excitation source may be a tungsten or xenon lamp, or a pulsed or continuous laser. The sample is typically either a thin film in a vacuum chamber (as shown here) or a solution in a cuvette. Optical components such as lens systems or glass fiber bundles direct the excitation and emission of light. The emitted light is detected after dispersion.

onto the sample, which may be a film on a substrate or a solution in a cuvette. The light emitted from the sample is then dispersed by a monochromator and detected using a photomultiplier tube or a photodiode. Such fluorescence spectrometers provide a convenient means to measure a large number of samples in a short space of time. When using them for thin-film measurements, care should be taken that the sample space containing the film is well purged with nitrogen to avoid accidental photooxidation of the sample. Solutions should be well dilute, preferably at concentrations below $10^{-6}$ mol of chromophore per liter of solvent, to avoid self-absorption (Figure 1.35). Self-absorption happens if light emitted from a higher-energy chromophore is reabsorbed by a lower-energy chromophore. (Keep in mind that the energy of chromophores varies slightly due to interactions with the solvent as detailed in Chapter 2 so that there is always a distribution of chromophores at different energies present in a sample.) In a spectrum, self-absorption can be identified if the energetic spacing between the 0–0 and 0–1 peaks

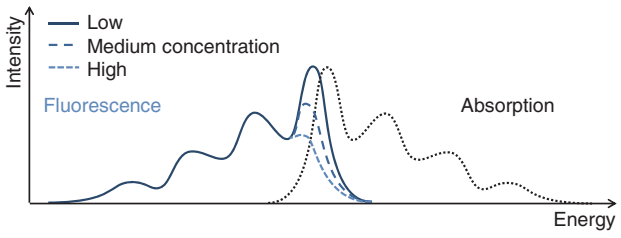


**Figure 1.35** Schematic illustration of the spectral changes associated with self-absorption. The increased re-absorption of emitted light when the sample is more concentrated reduces the intensity of the 0–0 vibrational peak and leads to an apparent shift of the peak position to lower energies.

reduces with increasing concentration, while the spacing from the 0–1 to 0–2 peaks remains constant.

The advantages of a home-made setup are a larger flexibility in the choice of excitation and detection components and a precise control over the measurement geometry. Instead of a monochromated xenon or deuterium lamp, one may use continuous-wave lasers (argon-ion lasers, helium–cadmium lasers, or solid-state lasers) which deliver high excitation intensities albeit at discrete wavelengths. For temperature control, the sample may be placed in a nitrogen or helium cryostat, preferably in vacuum or alternatively in an inert gas to prevent photo-oxidation. The traditional time-consuming method of detecting the emitted light with a photomultiplier behind a monochromator and then scanning the monochromator through a wavelength range is largely replaced by the use of a spectrograph in front of a charge-coupled device (CCD) camera. A monochromator and a spectrograph both consist of a box with grating in it that disperses the incoming light. The only difference is that a monochromator has a small exit slit so that the exiting light has a narrow wavelength range of 1 nm or less, while a spectrograph has a wide exit hole that yields a dispersed band of light which may be as wide as 400 nm. A CCD camera has a detector array. When the dispersed light band falls onto the detector array, each pixel records the light intensity of a particular wavelength interval. For example, if 400 nm is mapped onto 1240 pixels, each pixel roughly records the intensity from a 0.3-nm interval. The intensities obtained by the different pixels can be read out electronically, yielding the spectrum immediately.

When time-integrated spectra are recorded, one measures the emission from the state with the highest quantum yield. For organic compounds, this is the fluorescence from the $S_1$ state. In organometallic complexes, this is mostly the phosphorescence from $T_1$. When the spectral shape changes as a function of temperature, for example when heating from 10 K to room temperature, then this reflects a temperature activation of a transition rate between two states. This can be a temperature-dependent change between emission from two different conformations of a molecule, or between emission from a monomeric state and an excimer state, or between fluorescence and phosphorescence, or between a donor and an acceptor molecule, provided the energy transfer requires thermal activation.

To measure the photoluminescence quantum yield (PL QY) of a thin film, one needs to know the number of absorbed photons and the number of photons that are emitted from the film in any direction. This is best obtained by placing the film in the middle of a nitrogen-purged sphere that is coated with a diffuse, uniformly reflective paint. Such a sphere is called Ulbricht sphere or integrating sphere. The emitted light hitting the surface of the

sphere is reflected multiple times. This creates a uniform photon flux in the sphere that is independent of the initial direction in which the light was emitted. A first-order estimate of the quantum yield can be obtained from a sequence of two measurements. First, a small laser beam is let into the empty sphere through a small hole. Through another small hole, the spectrum in the sphere due to the scattered laser light is collected using a glass fiber coupled to a spectrograph and a CCD camera. It shows an intense peak at the laser wavelength. Next, the sample is placed in the middle of the sphere, and the laser is directed to hit the sample. Again, the spectrum of the scattered light is collected. It shows the light emitted by the sample as well as the scattered laser light. The intensity of the peak by the laser is now reduced since some of the laser light had been absorbed by the sample. The difference in the area under the laser peak measured with and without the sample in the integrating sphere corresponds to the number of absorbed photons. The area under the spectrum in the wavelength region where the sample emits gives the number of emitting photons. The ratio of the emitted photons to the absorbed photons is the quantum yield. The principle of this measurement is easy. For an accurate measurement on thin films, however, one needs to correct for the fact that some of the laser light is initially reflected from the sample, then reflected from the surface of the sphere, and then absorbed by the sample. This is done by a third measurement with the sample inside the sphere, and the laser hitting the surface of the sphere (not the sample). For the detailed mathematical treatment, we refer to Ref. [170] (Figure 1.36).

While the principle of this quantum yield measurement is simple, a few things need to be attended to. First, to determine the quantum yield with good accuracy, the third measurement that corrects for absorption of the scattered laser light is essential. There are meanwhile fluorescence spectrometers available that offer integrating sphere measurements. Some of them do not correct for reabsorption. Second, the sphere needs to be well-purged with nitrogen to avoid photooxidation in the case of fluorescence measurement and to avoid triplet state quenching for phosphorescence measurements (Box 1.14). Third, it is recommendable to take the measurement at a range of excitation intensities, starting from very low ones. The results are trustworthy as long as the numbers obtained for different excitation intensities match. When the quantum yield starts reducing with increasing excitation power, unwanted bimolecular process takes place and the quantum yield is no longer reliable, even though the signal-to-noise ratio may be better. Finally, this experiment relies on dividing two quantities, i.e. the number of emitted photons by the number of absorbed photons. When the exciting laser is very blue, such as at 405 nm or even shorter wavelength, the detecting unit (CCD camera or photodiode) may operate at the border of its measurement range. The number of absorbed photons is then determined with significant error, and the resulting quantum yield needs to be viewed with caution. This can, of course, be avoided by appropriate detector choice.

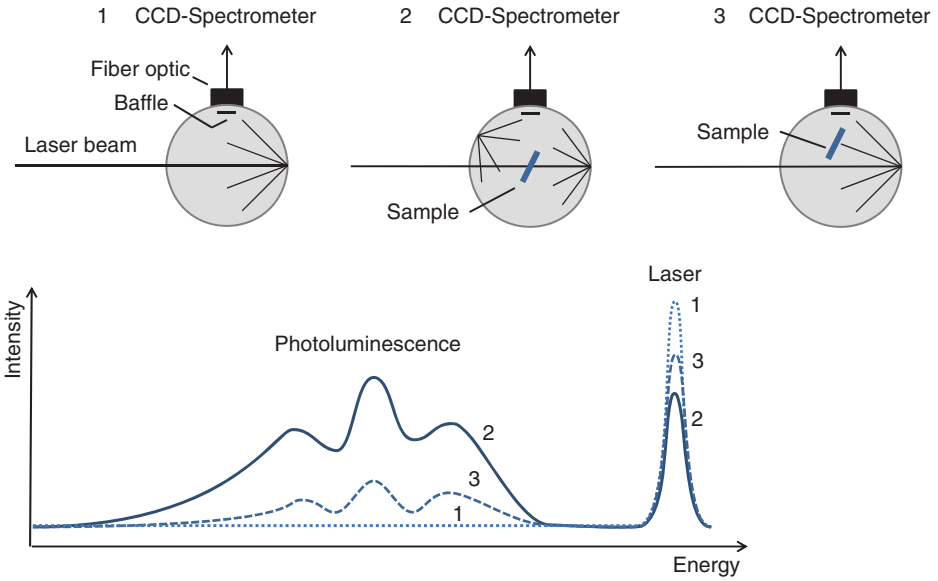


**Figure 1.36** Illustration of the measurements conducted to measure PL QY showing the configuration of the sphere (top) and the spectrum obtained (bottom). First, the laser is directed into the empty sphere (1), giving the photon flux at the laser wavelength (light blue dotted line). Next, the sample is placed in the sphere and excited (2), giving the photon flux of fluorescence and the flux of the incident laser photons reduced by the absorbed laser photons (dark blue solid line). Finally, the spectrum is recorded with the sample inside the sphere yet placed off-centre, so that the laser beam misses the sample (3). This allows to correct for absorption and emission effects due to scattered laser light (blue dashed line). (After [170].)

**Box 1.14 Quenching by Oxygen**

Molecular oxygen, $O_2$, is a very efficient quencher for phosphorescence. The HOMOs of the oxygen molecule are two antibonding degenerate π-orbitals so that the electronic ground state formed is a triplet state $T_0$. (Figure B1.14.1) The next higher excited states are two singlet states, $S_1$ and $S_2$, with energies of 0.98 eV and a 1.63 eV above the ground state and associated excited state lifetimes of 2700 and 7 s, respectively. The first optically allowed transition is to a triplet state at 6.2 eV [107]. The $T_0$, $S_1$, and $S_2$ states are frequently denoted by the spectroscopic symbols for diatomic molecule, in this case $^3\Sigma$, $^1\Delta$ and $^1\Sigma$, respectively. The indexes 3 and 1 denote the triplet or singlet state, and the Greek letter Σ or Δ indicates the angular momentum of the molecular state along the O–O axis, analogous to the terms s and d for the angular momentum of atomic states.

When a chromophore molecule in an excited triplet state, $^3M^*$, is adjacent to an oxygen molecule in the triplet ground state, $^3O_2$, energy transfer can take place. This results in an oxygen molecule in an excited singlet state ("singlet oxygen"), $^1O_2^*$, and a chromophore molecule in the ground state, $^1M$, so that phosphorescence is no longer possible. This process may be written as

$$^3M^* + {}^3O_2 \rightarrow {}^1M + {}^1O_2^* \qquad \text{(B1.14.1)}$$

Since the energy level of singlet oxygen is at only 0.98 eV, this mechanism can quench most of the triplet states encountered in organic semiconductors. Singlet oxygen is chemically very reactive during its lifetime and may attack the π-bonds in organic semiconductors. This reduces the luminescence efficiency of a material and the lifetime of an OLED made with it. A common reaction, e.g. for polyacenes, is a peroxidation reaction of the type $^1M + {}^1O_2^* \rightarrow MO_2$. In the case of anthracene peroxide, the oxygen molecule bridges the (9, 10-) positions of the anthracene molecule. Other well-known defects due to the reaction of (singlet or triplet) oxygen with organic semiconductors include the formation of keto defects (C=O), e.g. when breaking the vinyl bond in PPV, or when transforming a fluorene unit with incomplete sidechains into a fluorenone. Polyfluorenes containing such a fluorenone defect show a broad emission at 2.3 eV (540 nm), in addition to the reduced usual structured emission at 2.9 eV (420 nm) (Figure B1.14.2).

In passing, we note that ground state triplet oxygen may quench not only phosphorescence, but also fluorescence. Furthermore, it is well established that chemical defects in π-conjugated compounds occur in particular when the sample is exposed to oxygen and UV light simultaneously. A photoexcited molecule is more reactive than a molecule in the ground state and may react with the electronegative oxygen comparatively easily. This is in particular true for photoexcited π-systems, where electrons are only weakly bound. A good practice

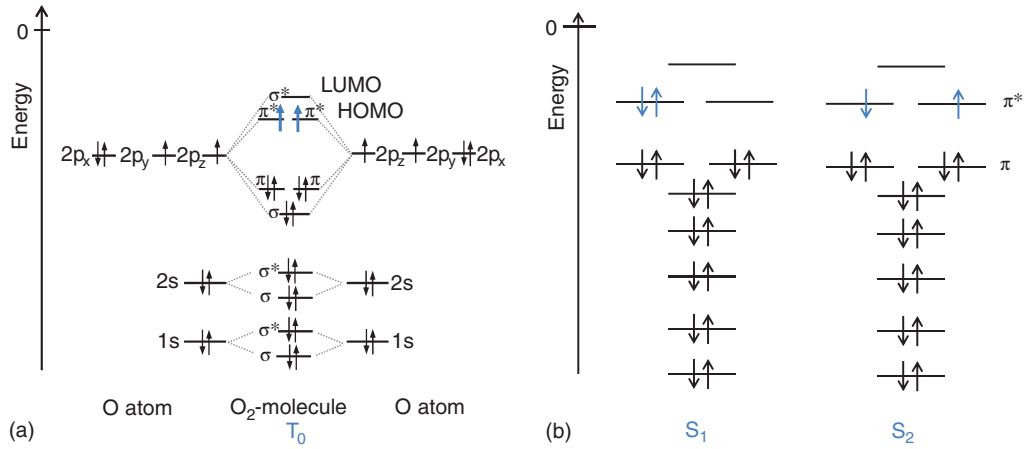


**Figure B1.14.1** (a) Simple molecular orbital (MO) diagram showing how interaction of two oxygen atoms results in the triplet ground state of $T_0$ $O_2$. Note that the two degenerate HOMOs occupied by one electron each are antibonding π-orbitals. (b) Simple MO diagram of the first and second singlet excited state of $O_2$. Electron spins in HOMOs are shown as blue arrows, all others as black arrows.

**Box 1.14 (Continued)**

is therefore to store samples in a dark, oxygen free atmosphere, e.g. in nitrogen, and to remove any residual oxygen prior to any optical measurement.

Techniques to remove oxygen from a sample involve keeping the sample under vacuum for an extended period in case of a film. For a solution, oxygen can be removed effectively by freezing the solution in a closed cuvette and then pumping off the oxygen that has been released as a gas into the space above the frozen solution. Then close the valve to the pump, bring the solution to room temperature and repeat the procedure several times. The alternative method of bubbling an inert gas such as nitrogen through the solution from a needle connected to a nitrogen line for a certain time is not as efficient.

More information on the photophysics and photochemistry of molecular oxygen may be found in [107, 112].

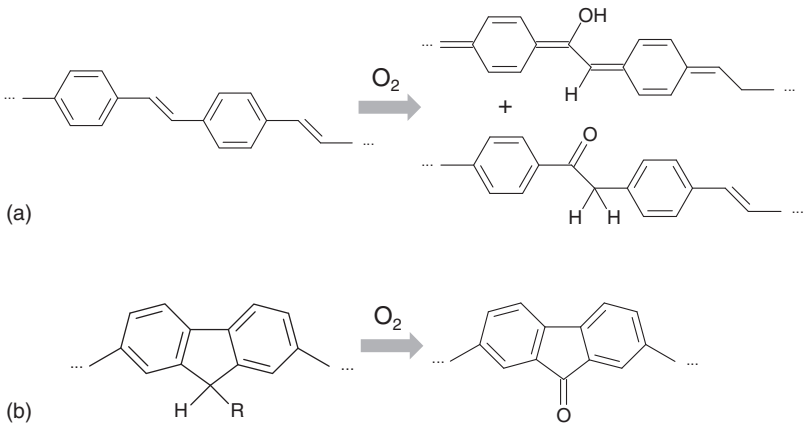


**Figure B1.14.2** Defects introduced by molecular oxygen (a) at poly(para-phenylene vinylene) (PPV), after [171] (b) at a fluorene unit in a poly(fluorene). R may be any alkyl group, for example, $C_8H_{17}$ (After List *et al.* [172].)

#### 1.5.1.2 Spectra and Lifetimes in the Nanosecond to Second Range

In organic compounds, phosphorescence cannot be measured by a steady state measurement due to the low phosphorescence rate. Instead, the excitation source needs to be a pulsed laser such as a Nd:YAG laser with ns pulses or a pulsed xenon lamp, both operated at 10 Hz or lower frequency (to avoid re-excitation before the triplet has entirely decayed). The detection unit consists of a spectrograph coupled to a gated intensified CCD camera (iCCD). After the excitation pulse, one waits until all of the fluorescence has decayed, typically a few ns. Then the detector gate is opened and left open for a sufficiently long time to collect any of the few photons possibly emitted from the triplet state. This may take between a microsecond and a few seconds, depending on the phosphorescence rate. The read-out of the detector array then yields the phosphorescence spectrum. Sometimes, one observes an additional signal that is identical to the steady state fluorescence in spectral shape and wavelength range, even though the delay time between laser pulse and detection far exceeds the fluorescence lifetime, and this additional signal may have a long lifetime such as a few microseconds. In this case, the $S_1$ state has been repopulated from a long-lived state such as the $T_1$ state or a charge-transfer state, and the emission is referred to as *delayed fluorescence*. In the recent literature, obtaining delayed fluorescence from $T_1$ has also been described as *nonresonant triplet up-conversion* [173–175]. Different mechanisms that cause delayed fluorescence are discussed in Chapter 3.

The lifetime of the phosphorescence (or any other type of luminescence) can be determined by measuring the decay of the luminescence intensity as a function of time and fitting this to an exponential decay function

$$I(t) = I_0 \exp\left(-\frac{t}{\tau}\right) + c \tag{1.86}$$

where $c$ is the baseline given by the detector noise level. To this end, one excites the sample with a ns pulse. The emitted light is dispersed through a monochromator and detected by a photomultiplier connected to an oscilloscope, which records the decay curve. Alternatively, the emitted light is recorded as a spectrum, by using a spectrograph coupled to iCCD, and the delay time between pulse and detection window is shifted stepwise (with a step width exceeding the gate width to avoid overlap). The intensity at a particular wavelength is then read off the spectrum for different delay times, and by this the decay curve is constructed. Sometimes, there are two distinct decay channels by which an

excited state can decay. In this case, the use of a biexponential decay curve

$$I(t) = I_1 \exp\left(-\frac{t}{\tau_1}\right) + I_2 \exp\left(-\frac{t}{\tau_2}\right) + c \qquad (1.87)$$

can be appropriate. The two lifetimes $\tau_1$ and $\tau_2$ should then always be quoted in combination with the two amplitudes $I_1$ and $I_2$, as the four quantities are not independent of each other. Fitting more than two exponentials to a nonmono-exponential decay curve rarely has any physical meaning. In disordered organic semiconductors, there frequently is a statistical distribution of radiative or nonradiative transition rates, and subsequently of lifetimes. This is the case, for example, when there is energy transfer to an acceptor or quencher that is randomly distributed in the sample. When a Gaussian distribution function is convoluted with an exponential decay function, this leads to a functional dependence known as stretched exponential,

$$I(t) = I_0 \exp\left(-\left[\frac{t}{\tau_1}\right]^{\alpha}\right) + c \qquad (1.88)$$

as illustrated in (Figure 1.37) [176–178]. It is convenient to display Eq. (1.81) on a double logarithmic plot as $\ln(\ln(I_0/I(t)))$ against $\ln(t/t_0)$, which gives a straight line with slope α. This form is also known as *Kohlrausch–Williams–Watt plot*. For $\alpha = 1$, a mono-exponential decay is recovered, while $\alpha = 1/2$, 1/3 and 1/6 can indicate a 3D, 2D and 1D energy transfer process, respectively, to a random distribution of acceptors (see also Förster transfer in Section 3.2.3, as well as Figure 3.57) for an experimental example).

When the decay occurs over many orders of magnitude in time and intensity, displaying the photoluminescence intensity on a log-log scale is particularly appropriate. This is, for example, the case for thermally activated delayed fluorescence (TADF) that consists of a prompt fluorescence (PF) decay with $\tau_{PF}$ in the timescale of a few nanoseconds to about 100 ns and a delayed fluorescence (DF) decay with $\tau_{DF}$ in the microsecond timescale. Both, the prompt and delayed components, can be effectively fitted using exponentials. A simple biexponential fit, as described by Eq. (1.82) (with $I_1 = I_{PF}$, $\tau_1 = \tau_{PF}$, $I_2 = I_{DF}$ and $\tau_2 = \tau_{DF}$), is usually sufficient to describe the luminescence intensity decay of TADF materials in solution (as illustrated in Figure 1.37). In contrast, in amorphous films, the emission may be more complex. Frequently, the emitter prevails with a distribution of molecular conformations, and hence a distribution of reverse intersystem crossing rates, leading to a multiexponential luminescence decay. The delayed fluorescence in such disordered films can be effectively fitted using a stretched exponential (as given in Eq. (1.83) or, as proposed by Monkman *et al.* [179] by describing the delayed fluorescence decay through a Riemann sum of statistical distribution of $N$ single exponential decays, each with decay rate $k_{DF}$ and initial amplitude $I_n$

$$I(t) = \sum_{n=1}^{N} I_n e^{-k_{DF}t} \xrightarrow{N\to\infty} \int_0^{\infty} \rho(k_{DF}) e^{-k_{DF}t} \mathrm{d}k_{DF} \qquad (1.89)$$

In Eq. (1.84), each summed exponential term represents the delayed fluorescence decay of subsets of TADF molecules in the film, each associated with a specific reverse intersystem crossing rate. In the limit of continuous $k_{DF}$, this form converges with the Laplace transform of a rate distribution function $\rho(k_{DF})$. Consequently, Eq. (1.84) can be employed to fit the luminescence decay curve, facilitating the extraction of the distribution of delayed fluorescence rates ($k_{DF}$) and associated lifetimes.

#### 1.5.1.3 Spectra and Lifetimes in the Picosecond to Nanosecond Range

To measure the time evolution of fluorescence spectra, one excites using a fast pulse such as a 100 fs pulse from a Ti:Sapphire laser. The emission can be detected using a spectrograph with *streak camera* attached. Similar to the case of a CCD camera, a wide band of emitted light falls onto the camera, thus providing the spectral dispersion required. The light falls onto a photocathode where it hits out electrons. Under the influence of a (horizontal) electric field, the electrons move to a counter electrode that is covered with a phosphor, just as in a cathode ray tube. To obtain the temporal dispersion needed, one applies a vertical electrical field that increases with time (the "streak"), as in an oscilloscope. The first photons to arrive at the camera will experience only a small vertical electric field and will be deflected little, while the photons arriving later will be subjected to a larger vertical field, resulting in a larger deflection. In this way, a two-dimensional picture is created on the phosphor, with the horizontal axis corresponding to the wavelength dispersion and the vertical axis mapping the temporal dispersion. Behind the phosphor, there is a two-dimensional CCD array to read out the signal intensity at each point. The resulting data is three dimensional and is usually displayed as a color-coded two-dimensional picture. The abscissa displays the wavelength range, the ordinate gives the time range, and the color or grayscale encodes the intensity (Figure 1.38). From this, the spectrum at a specific time and the decay curve at a specific wavelength can be readily extracted.

A different technique to record the decay curve is *time-correlated single-photon counting* (TCSPC). Here, the sample is excited with a pulsed diode laser at low intensity. After the excitation pulse, a timer counts the time until the detector (a photomultiplier tube after a monochromator)

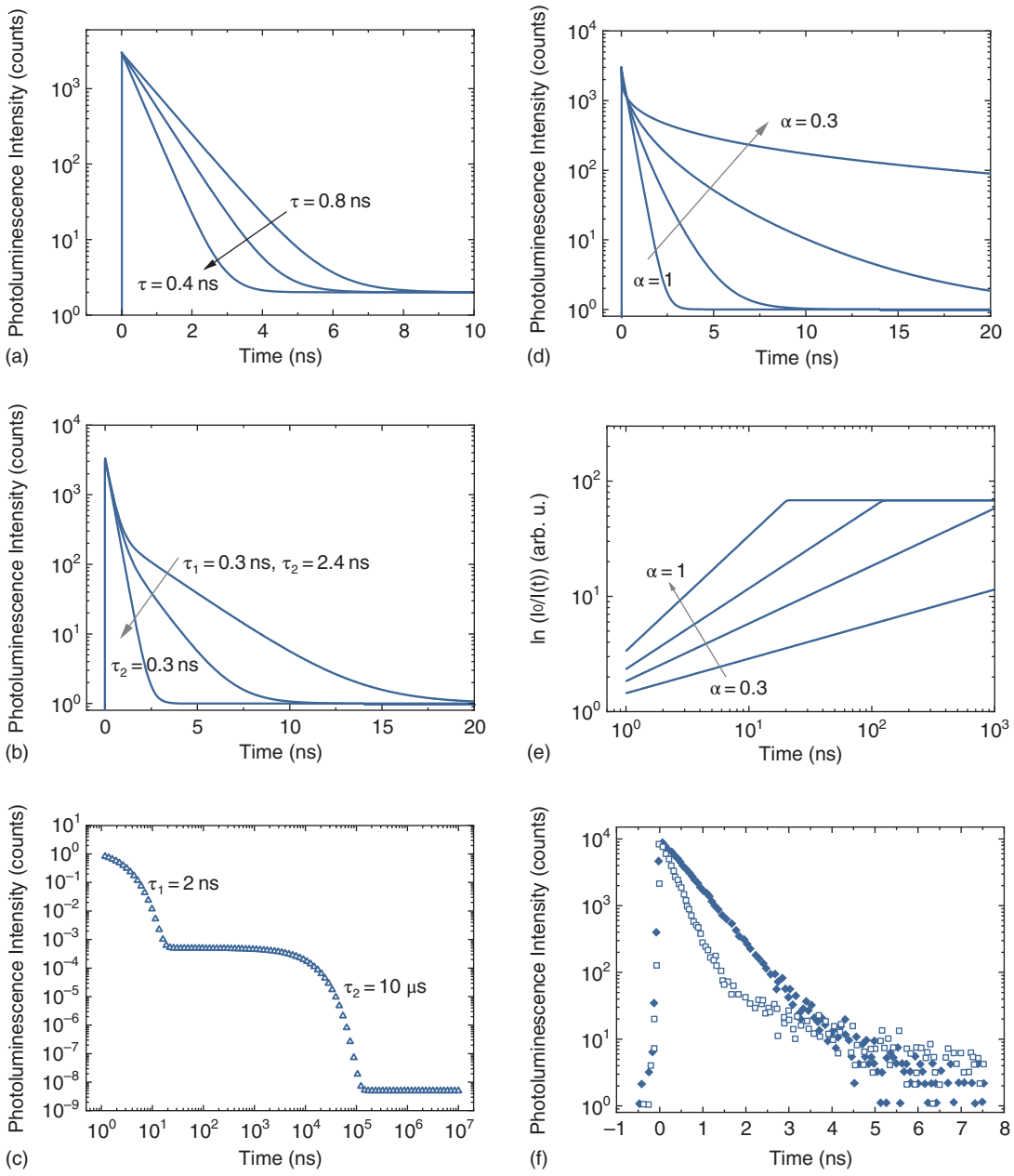


**Figure 1.37** Luminescence decay curves.
(a) Semilogarithmic plot of a mono-exponential decay (Eq. (1.81)) with $\tau = 0.8$, 0.6, and 0.4 ns.
(b) Semilogarithmic plot of a biexponential decay (Eq. (1.82)) with $(\tau_1, I_1)$ kept at (0.3 ns, $3 \times 10^3$) and $(\tau_2, I_2)$=(0.3 ns, $0.3 \times 10^3$), (1.2 ns, $0.3 \times 10^3$), and (2.4 ns, $0.3 \times 10^3$), respectively.
(c) Double-logarithmic plot of a biexponential decay (Eq. (1.82)) with $(\tau_1, I_1) = (2\text{ ns}, 1)$ and $(\tau_2, I_2) = (10\,\mu\text{s}, 1 \times 10^{-3})$.
(d) Semilogarithmic plot of a stretched exponential (Eq. (1.83)) with $\tau =$ and $\alpha = 0.3$, 0.5, 0.7, and 1.
(e) Kohlrausch-Williams-Watts (KWW) plot of the same stretched exponentials. Note that the $\ln(I_0/I(t))$ is plotted on a logarithmic axis, i.e. the inverse of the PL signal is shown in a double-log manner. The time is normalized to the start of measurement at $t_0$. The horizonal line at 80 is the constant c, corresponding to the baseline (noise level) of a measurement.
(f) Experimental example for a mono-exponential decay with $\tau_1 = 0.8$ ns (full symbols) and a biexponential decay with $(\tau_1, I_1) = (0.8\text{ ns}, 10^4)$ and $(\tau_2, I_2) = (1.7\text{ ns}, 10^2)$ and c = 1 (open symbols). The data is taken from a thin film at room temperature containing a fluorene trimer (full symbols) and a fluorene trimer doped with 2 mol% of an anthracene derivative (open symbols) (Data from Albuquerque *et al.* [105].)

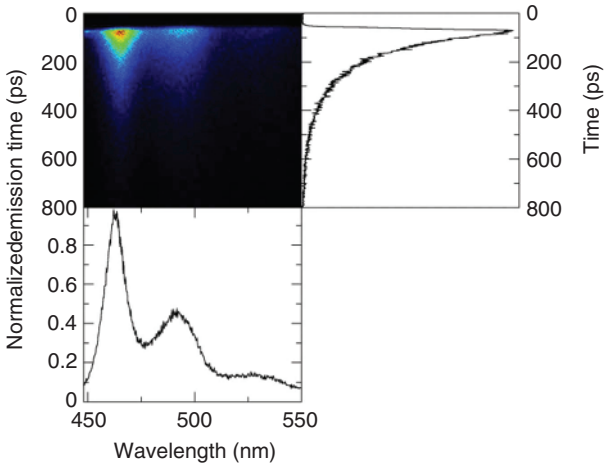


**Figure 1.38** Two-dimensional plot of a lifetime measurement. The abscissa indicates the wavelength, the ordinate indicates the time, and the color indicates the intensity. A cut at a fixed lifetime yields a spectrum, shown in the bottom. A cut at a fixed wavelength results in a decay curve, plotted on the right. The example shown here is for MeLPPP and was recorded using a spectrograph with a streak camera attached [180].

records the arrival of a single photon. This procedure is repeated many times. Displaying the number of photon counts against time then yields the decay curve. When this is done for multiple wavelengths, a spectrum can be constructed.

#### 1.5.1.4 Spectra and Time Scales Below the Picosecond Range

A technique to measure emission with spectral resolution below the picosecond time regime is *two-photon upconversion*. This experiment requires some knowledge and skill in nonlinear optics. A laser pulse, e.g. the 120 fs pulse from a Ti:Sapphire laser, is divided into two beams using a beam splitter. One beam (1) is used to excite the sample, and the emitted fluorescence is directed into a nonlinear optical crystal. The other beam (2) is directed over a longer light path to create a well-controlled time delay $\Delta t$ between beam 1 and beam 2 and then also enters the nonlinear crystal. Nonlinear crystals have the property that if a light with frequency $\omega_1$ and a light with frequency $\omega_2$ meet at the same time (and under the right angle), some light with the sum frequency $\omega_3 = \omega_1 + \omega_2$ is emitted. Thus, if beam 2 and the beam of the sample fluorescence meet at $\Delta t$ in the nonlinear crystal, light at a shifted frequency is emitted. This light can be dispersed by a spectrograph and recorded using a CCD camera to yield a spectrum. A high time resolution can be obtained by adjusting the time delay of beam 2 with respect to excitation beam 1. In a refined version of this experiment, no separate nonlinear crystal is employed. Rather, the organic semiconductor sample also acts as a nonlinear material.

### 1.5.2 Excited-State Absorption Spectra

The approach taken to measure the absorption from a molecule in the ground state has already been introduced in Section 1.4.2. Absorption can also occur from an excited state during the lifetime of that state. The only requirement is that the excited state absorption rate is higher than the excited state decay rate. This experiment requires two excitation sources. One source is used to illuminate the sample so as to create an excited state. For obvious reasons, this light beam is called the pump beam. The other source is employed to measure the absorption of the excited sample. This is the probe beam. Its attenuation by the sample is measured with a detector unit (Figure 1.39). Analogous to the photoluminescence measurements, different time regimes for this experiment require different excitation and detection equipment.

#### 1.5.2.1 Steady-State Spectra (Photoinduced Absorption)

When the probe beam is continuous, this technique is also called *photoinduced absorption* measurement and abbreviated with PiA or PA. The pump beam is typically an intense beam of about 100 mW/cm$^2$ from a laser such as an argon-ion laser. The sample is placed in vacuum to avoid photo-oxidation, or an oxygen-free solution is used (Box 1.14). The probe beam comes usually from a tungsten lamp. Tungsten lamps can run very stable and are particularly intense in the visible and near-infrared spectral range. This is just the range where the absorption features

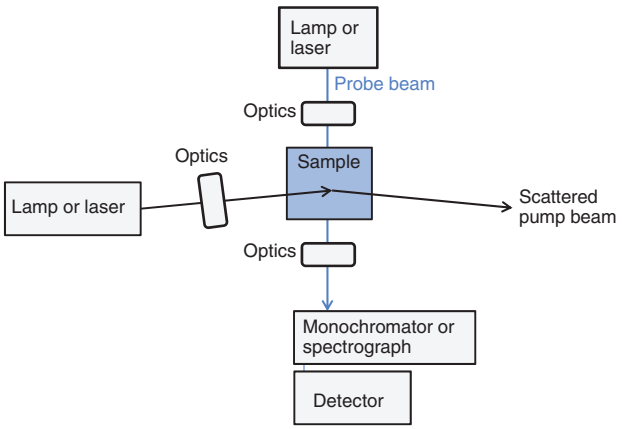


**Figure 1.39** A generic setup to measure photoinduced absorption. The sample (film or solution) may be excited ("pumped") using a continuous or pulsed laser. The absorption of the excited sample is recorded using a "probe" beam from a continuous tungsten lamp, a pulsed xenon lamp, or a pulsed white-light continuum from a laser and nonlinear crystal. The detector may be a CCD camera coupled to a spectrograph or, less frequently, a photodiode behind a monochromator. Time resolution can be obtained by using pulsed light sources and delaying the probe beam with respect to the pump beam.

from excited states tend to appear. The probe beam hits the sample normally to its surface and is transmitted. The transmitted light is directed into a monochromator, and the dispersed light is collected at the monochromator exit by a silicon photodiode or a similar detector. The quantity detected is the relative transmission with and without the pump beam, $\Delta T/T$, which is typically in the range of $\Delta T/T = 10^{-4}$. In order to measure the transmission with and without pump beam, $\Delta T$, a mechanical chopper is placed in the path of the pump beam, and the signal detected by the photodiode is recorded with a lock-in amplifier. To get a spectrum, the monochromator needs to be stepped through the desired wavelength range, and the PiA signal is recorded at each point. To normalize, a transmission spectrum without laser excitation, $T$, is also taken with the sample in the setup. No correction is required to account for the spectral response of the experimental setup as this is implicitly included when forming $\Delta T/T$.

With such a continuous-wave (cw) probe beam, the absorption features one measures are the ones from long-lived excited states such as triplet states, from charge-transfer states, or from charges that have been created after dissociation of an excited state. The $T_1 \rightarrow T_n$ transition is typically found around $1.5 \pm 0.2$ eV ($830 \pm 100$ nm) for semiconducting polymers and at higher energy for oligomers [157, 181] (Figure 1.40).

It is possible to measure the lifetime of these states by changing the frequency of the mechanical chopper and recording the change in signal intensity. When the period with ("on") and without ("off") pump beam becomes shorter than the decay time of the excited state, an excited-state population is still present in the "off" period. Consequently, the difference in transmission between the "on" and the "off" period reduces, and the lock-in detector records a drop in intensity. Dellepiane *et al*. used the rate equations for the photogenerated species to show that the intensity relates to the chopper frequency $\omega$ and excited-state lifetime $\tau$ as

$$I(\omega, \tau) = A \frac{\tau}{\sqrt{1 + (\omega\tau)^2}} \tag{1.90}$$

with A being a fitting constant [182]. This equation holds true for a monomolecular decay. Their paper also treats the bimolecular case. This method is limited to excited-state lifetimes of milliseconds and longer by the fact that mechanical choppers do not rotate stably beyond 4000 Hz.

#### 1.5.2.2 Spectra in the Nanosecond Range (Flash Photolysis)

The same measurement at higher time resolution is known as a transient absorption measurement or flash photolysis. It is a well-established technique that has been widely employed to record the transient absorption from triplet excited states or charged states in organic molecules, as its time resolution matches the lifetime of triplet and charged states. In this experiment, one uses a pulsed excitation source: for example, an Nd:YAG laser with 7 ns pulses at 10 Hz. The probe beam is typically a pulsed xenon lamp (a "flash lamp"). Operating the lamp in pulsed mode allows for high light intensities. The difference in transition from the xenon lamp with and without the laser pulse, normalized to the total transition, $\Delta T/T$, can now be obtained for different delay times between the pump beam and the probe beam, and this is what yields the time resolution of the measurement. Analogous to the case of emission measurements, two detection modes are possible. One may either record how the intensity of $\Delta T/T$ changes with time at a fixed wavelength by placing, for example, a Si-diode behind a monochromator, or one may take the spectrum of $\Delta T/T$ at a certain time after excitation by using a spectrograph coupled to an iCCD camera.

#### 1.5.2.3 Spectra in the Femtosecond Range (Femtosecond Pump-Probe Measurements)

A correspondingly higher time resolution is required for excited states with a shorter lifetime. As already mentioned, the time dependence in the measurement results from the time delay between the excitation (pump) pulse and the probe pulse. Of course, there is no point in having, say, a 300 fs delay between the pump and probe pulses if the pump pulse itself has a width of 7 ns. For a high time resolution, one therefore requires short pump pulses, such as pulses of about 100 fs duration supplied from a Ti:Sapphire laser. This laser emits around 800 nm, while most molecules require excitation in the blue spectral range. This can be arranged by sending a laser pulse with suitable polarization and incident angle through a nonlinear crystal (e.g. β-barium borate [BBO]). In the crystal, a nonlinear optical process converts incoming high-intensity light of one wavelength such as 800 nm into lower intensity light with half the wavelength, i.e. 400 nm (*frequency-doubling*). Next, one needs a probe beam with a well-defined delay with respect to the pump beam. This can be obtained by splitting the pump with a semitransparent mirror into two parts. Part one is still used as the pump beam and is directed onto the sample. Part two is employed as the probe beam. The time delay with respect to the pump is obtained by directing the probe beam over a longer optical path distance using mirrors. When the mirrors are set on translation stages (delay stage), control over the pump-probe time delay is easily reached by modifying the path length. For example, a total path difference of 15 cm between the pump and probe translates into a time delay of 500 fs, according to $\Delta x = c\Delta t$, with $c$ being the speed of light, $c = 3 \cdot 10\ \mathrm{ms}^{-1}$. With this,

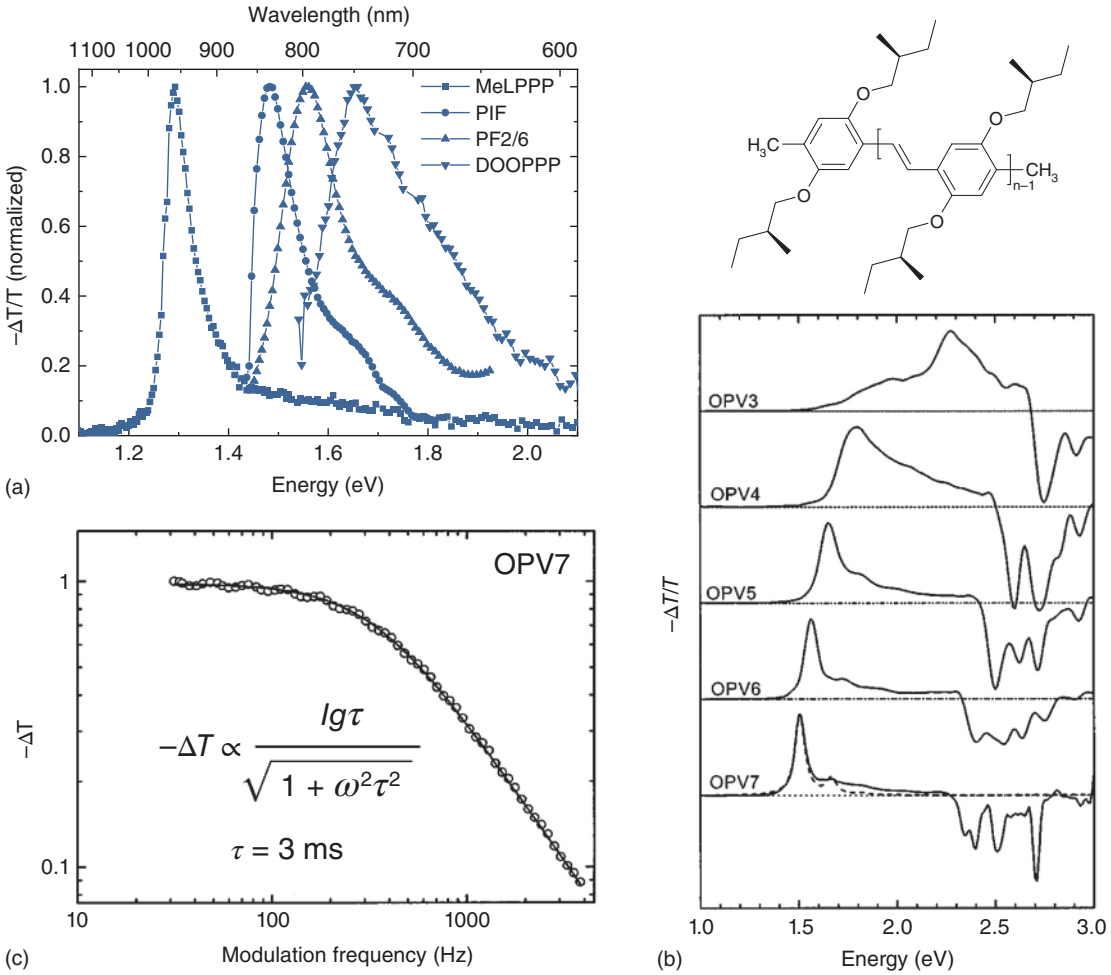


**Figure 1.40** Steady-state photoinduced absorption (a) of the $T_n \leftarrow T_1$ absorption in thin films of the polymers MeLPPP, PIF, PF, and DOOPPP, taken at 5 K and (b) of the $T_n \leftarrow T_1$ absorption at 1.5–2.3 eV of the OPVs shown above in MTH solutions at 100 K (From [157].) (c) Intensity dependence of the PIA band at 1.50 eV of OPV7 in 2MeTHF at 100 K as a function of the modulation frequency of the excitation beam, as well as a fit to the equation shown.

the setup consists of a short pump pulse and an equally short probe pulse with a well-defined delay time between them, but, unfortunately, also with the same wavelength. For a useful experiment, the probe beam needs to be at a different wavelength, preferably even dispersed to cover at a range of wavelengths. This can be obtained by directing the probe beam (at suitable polarization and incident angle) through a sapphire plate that, by a nonlinear optical process, disperses it into a beam with wavelengths covering the visible spectral range (*white light*). The UV pump beam now excites the sample, and at a fixed delay, the white-light probe beam is transmitted through it. The spectrum of the probe beam, with and without pump, is recorded by a CCD camera for different pump-probe delays. The time evolution of the signal at a particular wavelength is constructed by reading the intensity in the spectra taken at different times.

A typical example for a femtosecond pump-probe signal is shown in Figure 1.41 for a range of polymers. Changes in the absorption signal that occur upon pumping are illustrated in Figure 1.42 and include [183]

- a reduced absorption (*ground-state bleach*) (GSB) since some of the chromophores are still in an excited state, so they cannot absorb incident light,
- an additional absorption from the chromophore in the $S_1$ singlet excited state to a higher lying singlet excited state (*excited-state absorption*) (ESA or $PA_{S\text{-}EXC}$). At longer delay times, an additional absorption may also occur from the $T_1$ triplet excited state to a higher lying triplet state (ESA or $PA_{T\text{-}EXC}$),
- an additional absorption from a charged chromophore (*polaron absorption*) ($PA_{CS}$) that is formed when the $S_1$ state created by the pump pulse dissociates into positive and negative charges (see Chapter 2),

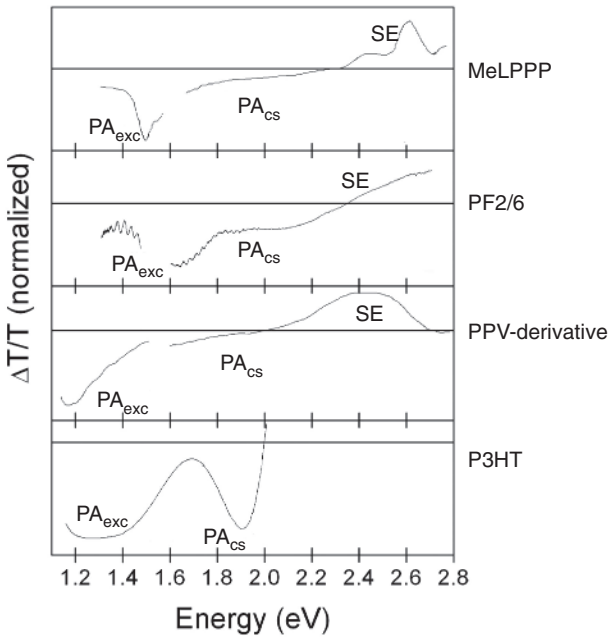


**Figure 1.41** The photoinduced absorption spectra of the polymers indicated taken with a pump-probe delay in the range of 100 fs–10 ps. (Figure from [183] with data from [184–187].) SE, PAcs, and PAexc denote the processes of stimulated emission, photoinduced absorption from a charged state, and photoinduced absorption from a (singlet or triplet) exciton, respectively.

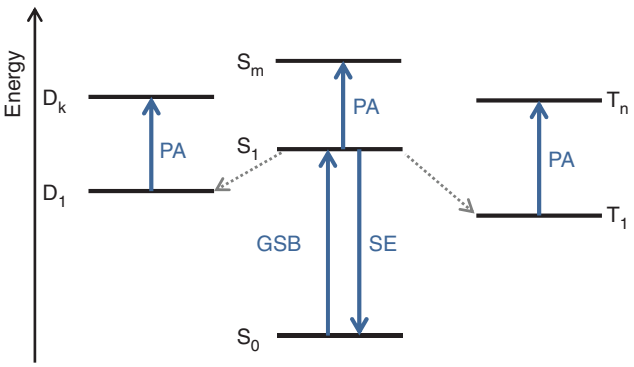


**Figure 1.42** Schematic of the different transitions that may be observed in pump-probe measurements (blue arrows). S, T, and D denote a singlet exciton, a triplet exciton, and a charged state (i.e. doublet spin), respectively. PA, SE, and GSB stand for photoinduced absorption, stimulated emission, and ground-state bleach, respectively. Dotted lines indicate nonradiative transitions after excitation.

- an additional photoluminescence (*stimulated emission*) (SE) that occurs because photons from the probe beam stimulate emission from the $S_1$ state generated by the pump beam.

While PA signals show up in the spectra as a reduction in the transmission (i.e. negative sign of $\Delta T/T$), SE and GSB signals give an increased transmission. The GSB is easily identified as it occurs at the wavelength of the usual absorption signal. Similarly, the SE coincides with the fluorescence spectrum. In polymers, PA signals from $T_n \leftarrow T_1$ transitions are frequently observed around $1.5 \pm 0.2$ eV, while PA signals from charges are common somewhere broadly around 2 eV and 0.5 eV (see also Chapter 2). A simple way to confirm the PA signal of a charged molecule is to dope the molecule extrinsically and to measure the normal, linear absorption spectrum for comparison (see Chapter 2). PA signals from triplet and singlet state absorption can be differentiated by their lifetime, with the triplet needing more time to form and more time to decay.

### 1.5.3 Fluorescence Excitation Spectroscopy

In a conventional absorption experiment, one measures the difference in the transmission of light beam with and without the absorber in the path of the light. For weak absorbers, this can become difficult. In that case, *fluorescence excitation spectroscopy* (FLE) is a helpful technique, provided that the sample is fluorescent. One detects the fluorescence of the sample as a function of the excitation energy. If the nonradiative decay from the sample is independent of excitation energy, then the emission intensity will be proportional to the absorption of the sample, and one obtains a direct portrait of the absorption spectrum. For some samples, a different nonradiative decay path may become accessible upon increasing the excitation energy. In that case, the FLE spectrum differs from the absorption spectrum, and concomitantly, this difference can be employed to identify such processes, which may include energy transfer processes or photodissociation.

When conducting the experiment, the measurement geometry needs to be selected with care to avoid artifacts from self-absorption. A geometry where the exciting laser beam hits the sample surface (film or cuvette) under a flat angle of incidence while the emitted luminescence is detected normally tends to work well (as illustrated in Figure 1.31). The standard geometry in commercial luminescence spectrometers, where a 1-cm cuvette of solution is excited and the luminescence is detected at 90° angle, only works for very dilute solutions and is particularly prone to self-absorption effects.

## 1.6 Further Reading

The electronic properties of organic semiconductors require knowledge from a wide range of fields. The topics just covered in this first chapter draw from the areas of synthetic chemistry, polymer science, crystallography, quantum mechanics, photophysics, and spectroscopy.

Subsequent chapters will further include issues from semiconductor physics, device physics, engineering, and material science. This book can merely give an introduction to the electronic properties of organic semiconductors. It aims to provide an initial orientation that allows the reader to follow up different threads in more depth. We list here some literature that may be useful to this purpose. By nature of being a selection, it is not comprehensive and it reflects our own preferences. The literature is listed in the context of the section that it substantiates further.

**Section 1.2 on Different Organic Semiconductor Materials:** More information about the structure of crystalline organic semiconductors can be found in the book by Schwoerer and Wolf, *Organic Molecular Solids* [22]. For a brief introduction to polymer physics, we recommend Chapter 2 in the book *Introduction to Soft Matter* by Hamley and Chapter 5 in the book *Soft Condensed Matter* by Jones [68], while more extensive treatment is given in the book *The Physics of Polymers* by Strobl [188]. Issues pertaining to the synthesis of semiconducting polymers are discussed in a number of edited books: for example, Chapters 1 and 2 in the book *Semiconducting Polymers*, edited by Hadziioannou and Malliaras [76].

**Section 1.3 on Electronic States of a Molecule:** The concepts of bonding, molecular orbitals, and states are very well explained in the books *Molecular Physics* by Demtröder and *Molecular Quantum Mechanics* by Atkins and Friedman [78, 79].

**Section 1.4 on Transitions Between Molecular States:** There are a number of books that introduce these topics. Pope and Swenberg, as well as Birks, have written the corresponding chapters of their books with a particular view to organic semiconductors, and both books may be considered as classic for those working in the field. The book by Birks, *Photophysics of Aromatic Molecules*, is highly recommendable [112]. Its only disadvantage is that it is out of print, though available in many scientific libraries. Pope and Swenberg's book *Electronic Processes in Organic Crystals and Polymer*s is available as a 2nd edition [21]. Another good introduction to transitions between molecular states can be found in *Modern Molecular Photochemistry of Organic Molecules* by Turro, Ramamurthy, and Scaiano, which is also available as a 2nd edition [116]. It has a strong emphasis on visualizing the photophysical and photochemical processes. A classic approach is given in *Excited States and Photochemistry of Organic Molecules* by Klessinger and Michl [189]. A clear and concise introduction can also be found in *Modern Spectroscopy* by Hollas [190].

**Section 1.5 on Spectroscopic Methods:** A detailed and practical introduction to the techniques of absorption and luminescence spectroscopy can be found in *Principles of Fluorescence Spectroscopy* by Lakowicz. The examples mostly use biologically relevant molecules [191]. A stronger focus on organic molecules and electronic transitions is given by Valeur in *Molecular Fluorescence* [192].

## References


1 Riede, M., Spoltore, D., and Leo, K. (2021) Organic solar cells—the path to commercial success. *Adv. Energy Mater.*, **11** (1), 2002653.

2 Liu, Y., Feig, V.R., and Bao, Z. (2021) Conjugated polymer for implantable electronics toward clinical application. *Adv. Healthcare Mater.*, **10** (17), 2001916.

3 Wang, W. *et al*. (2021) Strain-insensitive intrinsically stretchable transistors and circuits. *Nat. Electron.*, **4** (2), 143.

4 Lee, H. *et al*. (2017) Wearable/disposable sweat-based glucose monitoring device with multistage transdermal drug delivery module. *Sci. Adv.*, **3** (3), e1601314.

5 Wang, W. *et al*. (2023) Neuromorphic sensorimotor loop embodied by monolithically integrated, low-voltage, soft e-skin. *Science*, **380** (6646), 735.

6 Antognazza, M.R. *et al*. (2016) Characterization of a polymer-based, fully organic prosthesis for implantation into the subretinal space of the rat. *Adv. Healthcare Mater.*, **5** (17), 2271.

7 Ghezzi, D. *et al*. (2013) A polymer optoelectronic interface restores light sensitivity in blind rat retinas. *Nat. Photonics*, **7** (5), 400.

8 Ferlauto, L. *et al*. (2018) Design and validation of a foldable and photovoltaic wide-field epiretinal prosthesis. *Nat. Commun.*, **9** (1), 992.

9 Maya-Vetencourt, J.F. *et al*. (2017) A fully organic retinal prosthesis restores vision in a rat model of degenerative blindness. *Nat. Mater.*, **16** (6), 681.

10 Maya-Vetencourt, J.F. *et al*. (2020) Subretinally injected semiconducting polymer nanoparticles rescue vision in a rat model of retinal dystrophy. *Nat. Nanotechnol.*, **15** (8), 698.

11 Pochettino, A. (1906) Sul comportamento foto-elettrico dell' antracene. *Rendiconti*, **15**, 355.

12 Königsberger, J. and Schilling, K. (1910) Über Elektrizitätsleitung in festen Elementen und Verbindungen. *Ann. Phys.*, **32**, 179.

13 Stark, J. and Steubing, W. (1908) Fluorescence and light electrical sensitivity of organic substances. *Phys. Z.*, **9**, 481.

14 Pauli, W.E. (1913) Lichtelektrische Untersuchungen an fluoreszierenden Substanzen. *Ann. Phys.*, **345** (4), 677.

15 Bernanose, A., Comte, M., and Vouaux, P. (1953) A new method of emission of light by certain organic compounds. *J. Chim. Phys.*, **50**, 64.

16 Pope, M., Magnante, P., and Kallmann, H.P. (1963) Electroluminescence in organic crystals. *J. Chem. Phys.*, **38** (8), 2042.

17 Helfrich, W. and Schneider, W.G. (1965) Recombination radiation in anthracene crystals. *Phys. Rev. Lett.*, **14** (7), 229.

18 Helfrich, W. and Schneider, W.G. (1966) Transients of volume-controlled current and of recombination radiation in anthracene. *J. Chem. Phys.*, **44** (8), 2902.

19 Tang, C.W. and Vanslyke, S.A. (1987) Organic electroluminescent diodes. *Appl. Phys. Lett.*, **51** (12), 913.

20 Burroughes, J.H. *et al*. (1990) Light-emitting diodes based on conjugated polymers. *Nature*, **347**, 539.

21 Pope, M. and Swenberg, C.E. (1982) *Electronic Processes in Organic Crystals*, Clarendon Press, Oxford.

22 Schwoerer, M. and Wolf, H.C. (2007) *Organic Molecular Solids*, Wiley-VCH, Weinheim, ISBN: 9783527405404 3527405402.

23 Scher, H. and Montroll, E.W. (1975) Anomalous transit-time dispersion in amorphous solids. *Phys. Rev. B*, **12**, 2455.

24 Borsenberger, P.M. and Weiss, D.S. (1998) *Organic Photoreceptors for Xerography*, Marcel Dekker, New York.

25 Heeger, A.J. (2001) Semiconducting and metallic polymers: the fourth generation of polymeric materials (Nobel lecture). *Angew. Chem. Int. Ed.*, **40** (14), 2591.

26 Chiang, C.K. *et al*. (1977) Electrical-conductivity in doped polyacetylene. *Phys. Rev. Lett.*, **39** (17), 1098.

27 Su, W.P., Schrieffer, J.R., and Heeger, A.J. (1979) Solitons in polyacetylene. *Phys. Rev. Lett.*, **42** (25), 1698.

28 Su, W.P., Schrieffer, J.R., and Heeger, A.J. (1980) Soliton excitations in polyacetylene. *Phys. Rev. B*, **22** (4), 2099.

29 Sariciftci, E.N.S. (1997) *Primary Photoexcitations in Conjugated Polymers: Molecular Exciton Versus Semiconductor Band Model*, World Scientific, Singapor, ISBN: 978-9810228804.

30 Scaccabarozzi, A.D. *et al*. (2022) Doping approaches for organic semiconductors. *Chem. Rev.*, **122** (4), 4420.

31 Scholes, G.D. and Rumbles, G. (2006) Excitons in nanoscale systems. *Nat. Mater.*, **5**, 683.

32 Hong, G. *et al*. (2021) A brief history of OLEDs—emitter development and industry milestones. *Adv. Mater.*, **33** (9), 2005630.

33 Fratini, S. *et al*. (2020) Charge transport in high-mobility conjugated polymers and molecular semiconductors. *Nat. Mater.*, **19** (5), 491.

34 Silinsh, E.A. and Capek, V. (1994) *Organic Molecular Crystals*, AIP Press, New York, ISBN: 978-1563960697.

35 Wright, J.D. (ed.) (1995) *Molecular Crystals*, Cambridge University Press.

36 Kitaigorodskii, A.I. (1973) *Molecular Crystals and Molecules*, Academic Press, New York, ISBN: 978-0124105508.

37 Choi, H.H. *et al*. (2018) Critical assessment of charge mobility extraction in FETs. *Nat. Mater.*, **17** (1), 2.

38 Liu, C. *et al*. (2017) Device physics of contact issues for the overestimation and underestimation of carrier mobility in field-effect transistors. *Phys. Rev. Appl.*, **8** (3), 034020.

39 Sirringhaus, H. *et al*. (1999) Two-dimensional charge transport in self-organized, high-mobility conjugated polymers. *Nature*, **401** (6754), 685.

40 Cho, Y.-J. *et al*. (2017) Important role of ancillary ligand in the emission behaviours of blue-emitting heteroleptic Ir(iii) complexes. *J. Mater. Chem. C*, **5** (18), 4480.

41 Tamayo, A.B. *et al*. (2003) Synthesis and characterization of facial and meridional tris-cyclometalated iridium(III) complexes. *JACS*, **125** (24), 7377.

42 Koch, F.P.V. *et al*. (2013) The impact of molecular weight on microstructure and charge transport in semicrystalline polymer semiconductors–poly(3-hexylthiophene), a model study. *Prog. Polym. Sci.*, **38** (12), 1978.

43 Rothberg, L. (2006) Photophysics of conjugated polymers. in *Semiconducting Polymers* (eds G. Hadziioannou and G.G. Malliaras), Wiley-VCH, Weinheim, ISBN: 978-3-527-31271-9.

44 Ariu, M. *et al*. (2002) The effect of morphology on the temperature-dependent photoluminescence quantum efficiency of the conjugated polymer poly(9, 9-dioctylfluorene). *J. Phys. Condens. Matter*, **14** (42), 9975.

45 Silva, C. *et al*. (2002) Exciton and polaron dynamics in a step-ladder polymeric semiconductor: the influence of interchain order. *J. Phys. Condens. Matter*, **14** (42), 9803.

46 Hayer, A. *et al*. (2005) Morphology dependence of the triplet excited state formation and absorption in polyfluorene. *Phys. Rev. B*, **71** (24), 241302.

47 Mauer, R., Kastler, M., and Laquai, F. (2010) The impact of polymer regioregularity on charge transport and efficiency of P3HT:PCBM photovoltaic devices. *Adv. Funct. Mater.*, **20** (13), 2085.

**48** Scherf, U. and List, E.J.W. (2002) Semiconducting polyfluorenes -towards reliable structre-property relationships. *Adv. Mater.*, **14** (7), 477.

**49** Burn, P.L. *et al*. (1992) Precursor route chemistry and electronic-properties of poly(*p*-phenylene-vinylene), poly[(2,5-dimethyl-*p*-phenylene)vinylene] and poly[(2,5-dimethoxy-*p*-phenylene)vinylene]. *J. Chem. Soc. Perkin Trans.*, **1** (23), 3225.

**50** Png, R.Q. *et al*. (2010) High-performance polymer semiconducting heterostructure devices by nitrene-mediated photocrosslinking of alkyl side chains. *Nat. Mater.*, **9** (2), 152.

**51** Müller, C.D. *et al*. (2003) Multi-colour organic light-emitting displays by solution processing. *Nature*, **421** (6925), 829.

**52** Jandke, M. *et al*. (2001) Polarized electroluminescence from photocrosslinkable nematic fluorene bisacrylates. *SPIE Proc.*, **4105**.

**53** Scheler, E. and Strohriegl, P. (2010) Three color random Fluorene-based oligomers for fast micrometer-scale Photopatterning. *Chem. Mater.*, **22** (4), 1410.

**54** Prigodin, V.N. *et al*. (2008) Electron-ion interaction in doped conducting polymers. *Phys. Rev. B*, **78** (3), 035203.

**55** Lee, H.J., Lee, J., and Park, S.M. (2010) Electrochemistry of conductive polymers. 45. Nanoscale conductivity of PEDOT and PEDOT:PSS composite films studied by current-sensing AFM. *J. Phys. Chem. B*, **114** (8), 2660.

**56** Jung, J.W., Lee, J.U., and Jo, W.H. (2010) High-efficiency polymer solar cells with water-soluble and self-doped conducting polyaniline graft copolymer as hole transport layer. *J. Phys. Chem. C*, **114** (1), 633.

**57** Li, D., Huang, J.X., and Kaner, R.B. (2009) Polyaniline nanofibers: a unique polymer nanostructure for versatile applications. *Acc. Chem. Res.*, **42** (1), 135.

**58** Lee, K.H. *et al*. (1998) Nature of the metallic state in conducting polypyrrole. *Adv. Mater.*, **10** (6), 456.

**59** Hulea, I.N. *et al*. (2005) Doping, density of states, and conductivity in polypyrrole and poly(p-phenylene vinylene). *Phys. Rev. B*, **72** (5).

**60** Banerjee, S. and Kumar, A. (2010) Dielectric behavior and charge transport in polyaniline nanofiber reinforced PMMA composites. *J. Phys. Chem. Solids*, **71** (3), 381.

**61** MacDiarmid, A.G. (2001) "synthetic metals": a novel role for organic polymers (Nobel lecture). *Angew. Chem. Int. Ed.*, **40** (14), 2581–2590.

**62** Smela, E., Lu, W., and Mattes, B.R. (2005) Polyaniline actuators - part 1. PANI(AMPS) in HCl. *Synth. Met.*, **151** (1), 25–42.

**63** Kirchmeyer, S. and Reuter, K. (2005) Scientific importance, properties and growing applications of poly(3,4-ethylenedioxythiophene). *J. Mater. Chem.*, **15** (21), 2077.

**64** Kroto, H.W. *et al*. (1985) C-60 - buckminsterfullerene. *Nature*, **318** (6042), 162.

**65** Dresselhaus, M.S., Dresselhaus, G., and Eklund, P.C. (1993) Fullerenes. *J. Mater. Res.*, **8** (8), 2054.

**66** Dresselhaus, M.S., Dresselhaus, G., and Saito, R. (1995) Physics of carbon nanotubes. *Carbon*, **33** (7), 883.

**67** Dresselhaus, M.S., Dresselhaus, G., and Jorio, A. (2004) Unusual properties and structure of carbonnanotubes. *Annu. Rev. Mater. Res.*, **34**, 247.

**68** Hamley, I. (2007) *Introduction to Soft Matter*, Wiley-VCH, ISBN: 9780470516102.

**69** Chandrasekha, S. (1994) *Liquid Crystals*, Cambridge University Press, ISBN: 978-0521417471.

**70** Ding, L. *et al*. (2023) Polymer semiconductors: synthesis, processing, and applications. *Chem. Rev.*, **123** (12), 7421.

**71** Mccullough, R.D. and Lowe, R.D. (1992) Enhanced electrical-conductivity in regioselectively synthesized poly(3-Alkylthiophenes). *J. Chem. Soc. Chem. Commun.*, **1**, 70.

**72** Marrocchi, A. *et al*. (2012) Poly(3-hexylthiophene): synthetic methodologies and properties in bulk heterojunction solar cells. *Energy Environ. Sci.*, **5** (9), 8457.

**73** Yokoyama, A., Miyakoshi, R., and Yokozawa, T. (2004) Chain-growth polymerization for poly(3-hexylthiophene) with a defined molecular weight and a low polydispersity. *Macromolecules*, **37** (4), 1169.

**74** Lohwasser, R.H. and Thelakkat, M. (2011) Toward perfect control of end groups and polydispersity in poly(3-hexylthiophene) via catalyst transfer polymerization. *Macromolecules*, **44** (9), 3388.

**75** Bronstein, H. *et al*. (2020) The role of chemical design in the performance of organic semiconductors. *Nat. Rev. Chem.*, **4** (2), 66.

**76** Bolognesi, A. and Pasini, M.C. (2007) Synthetic methods for semiconducting polymers. in *Semiconducting Polymers* (eds G. Hadziioannou and G.G. Malliaras), Wiley VCH, Weinheim, ISBN: 978-3-527-31271-9.

**77** Kallitsis, J.K., Tsolakis, M.C., and Andreopoulou, A.K. (2007) Processable semiconducting polymers containing oligoconjugated blocks. in *Semiconducting Polymers* (eds G. Hadziioannou and G.G. Malliaras), Wiley VCH, Weinheim, ISBN: 978-3-527-31271-9.

**78** Atkins, P.W. (1983) *Molecular Quantum Mechanics*, 2nd edn, Oxford University Press.

79 Demtröder, W. (2005) *Molecular Physics*, Wiley-VCH, ISBN: 978-3527405664.

80 Atkins, P.W. and Friedman, R.S. (1996) *Molecular Quantum Mechanics*, 3rd edn, Oxford University Press, Oxford.

81 Demtröder, W. (2003) *Molekülphysik*, Oldenbourg Wissenschaftsverlag GmbH, München.

82 Miller, R.D. (1989) Polysilanes - a new look at some old materials. *Angew. Chem. Int. Ed. Engl.*, **28** (12), 1733.

83 Stolka, M. *et al*. (1990) Manifestation of glass-transition in electronic charge transport in Si and Ge backbone polymers. *Synth. Met.*, **37** (1-3), 295.

84 Bredas, J.L. (2014) Mind the gap! Materials. *Horizon*, **1**, 17.

85 Haken, H.W. and Wolf, H.C. (2006) *Molekülphysik und Quantenchemie*, Springer.

86 Yersin, H. and Finkenzeller, W.J. (2007) Triplet emitters for organic light-emitting diodes:basic properties. in *Highly efficient OLEDs with Phosphorescent Materials* (ed. H. Yersin), Wiley-VCH, ISBN: 978-3527405947.

87 Köhler, A. and Bässler, H. (2009) Triplet states in organic semiconductors. *Mater. Sci. Eng., R*, **66**, 71.

88 Hicks, R.G. (2007) What's new in stable radical chemistry? *Org. Biomol. Chem.*, **5** (9), 1321.

89 Power, P.P. (2003) Persistent and stable radicals of the heavier Main group elements and related species. *Chem. Rev.*, **103** (3), 789.

90 Cui, Z. *et al*. (2020) Stable luminescent radicals and radical-based LEDs with doublet emission. *CCS Chem.*, **2** (4), 1129.

91 Gamero, V. *et al*. (2006) [4-(N-Carbazolyl)-2,6-dichlorophenyl]bis(2,4,6-trichlorophenyl)methyl radical an efficient red light-emitting paramagnetic molecule. *Tetrahedron Lett.*, **47** (14), 2305.

92 Kasemthaveechok, S. *et al*. (2022) Organic radicals with inversion of SOMO and HOMO energies and potential applications in optoelectronics. *Chem. Sci.*, **13** (34), 9833.

93 Hudson, J.M., Hele, T.J.H., and Evans, E.W. (2021) Efficient light-emitting diodes from organic radicals with doublet emission. *J. Appl. Phys.*, **129** (18).

94 Ai, X. *et al*. (2018) Efficient radical-based light-emitting diodes with doublet emission. *Nature*, **563** (7732), 536.

95 Peng, Q. *et al*. (2015) Organic light-emitting diodes using a neutral π radical as emitter: the emission from a doublet. *Angew. Chem. Int. Ed.*, **54** (24), 7091.

96 Guo, H. *et al*. (2019) High stability and luminescence efficiency in donor–acceptor neutral radicals not following the Aufbau principle. *Nat. Mater.*, **18** (9), 977.

97 Abdurahman, A. *et al*. (2020) Understanding the luminescent nature of organic radicals for efficient doublet emitters and pure-red light-emitting diodes. *Nat. Mater.*, **19** (11), 1224.

98 Johnston, M.B. *et al*. (2003) Low-energy vibrational modes in phenylene oligomers studied by THz time-domain spectroscopy. *Chem. Phys. Lett.*, **377** (1-2), 256–262.

99 Karabunarliev, S. *et al*. (2000) Rigorous Franck-Condon absorption and emission spectra of conjugated oligomers from quantum chemistry. *J. Chem. Phys.*, **113** (24), 11372–11381.

100 Mariani, M.M. and Deckert, V. (2012) Raman spectroscopy: principles, benefits & applications. *Bunsen-Magazin*, **4**, 136–147.

101 Hollas, J.M. (1992) *Modern Spectroscopy*, 2nd edn, John Wiley & Sons Ltd., Chichester.

102 Khan, A.L.T. (2005) Analysis of electron-phonon coupling from the luminescence of conjugated polymers. in *Cavendish Laboratory*, University of Cambridge, Cambridge, UK.

103 Köhler, A. *et al*. (2012) The role of C-H and C-C streching modes in the intrinsic non-radiative decay of triplet states in a Pt-containing conjugated phenylene ethynylene. *J. Chem. Phys.*, **136**, 094905.

104 Liu, Y. *et al*. (2002) Photophysics of monodisperse platinum-acetylide oligomers: delocalization in the singlet and triplet excited states. *JACS*, **124** (42), 12412–12413.

105 Albuquerque, R.Q. *et al*. (2011) Diffusion-limited energy transfer in blends of oligofluorenes with an anthracene derivative. *J. Phys. Chem. B*, **115** (25), 8063–8070.

106 Sandee, A.J. *et al*. (2004) Solution-processible conjugated electrophosphorescent polymers. *J. Chem. Am. Soc.*, **126** (22), 7041.

107 Turro, N.J. (1991) *Modern Molecular Photochemistry*, 2nd edn, University Science Books, Sausalito/California.

108 Kearwell, A. and Wilkinson, F. (1969). Chemistry of electronically excited states of organic molecules. in *Transfer and Storage of Energy by Molecules* (Vol. 1) (eds Q.M. Burnett and A.M. North), Wiley, New York.

109 Strickler, S.J. and Berg, R.A. (1962) Relationship between absorption intensity and fluorescence lifetime of molecules. *J. Chem. Phys.*, **37** (4), 814.

110 Kahle, F.-J. *et al*. (2018) How to interpret absorption and fluorescence spectra of charge transfer states in an organic solar cell. *Mater. Horiz.*, **5** (5), 837.

111 Siebrand, W. (1967) Radiationless transitions in polyatomic molecules. I. Calculation of Franck-Condon factors. *J. Chem. Phys.*, **46** (2), 440–447.

**112** Birks, J.B. (1970) *Photophysics of Aromatic Molecules*, Wiley-Interscience, London.

**113** Wilson, J.S. *et al*. (2003) Polarization of singlet and triplet excited states in a platinum-containing conjugated polymer. *Phys. Rev. B*, **67** (12), 125206.

**114** King, S.M., Vaughan, H.L., and Monkman, A.P. (2007) Orientation of triplet and singlet transition dipole moments in polyfluorene, studied by polarised spectroscopies. *Chem. Phys. Lett.*, **440** (4-6), 268.

**115** Lupton, J.M. *et al*. (2002) Intrinsic room-temperature electrophosphorescence from a pi-conjugated polymer. *Phys. Rev. Lett.*, **89** (16), 167401.

**116** Turro, N.J. (1965) *Molecular Photochemistry. Frontiers in Chemistry*, W.A. Benjamin, New York, xiii 286 p.

**117** Mcglynn, S.P. *et al*. (1962) External heavy-atom spin-orbital coupling effect. 3. Phosphorescence spectra and lifetimes of externally perturbed Naphthalenes. *J. Phys. Chem.*, **66** (12), 2499.

**118** Mcglynn, S.P., Kasha, M., and Azumi, T. (1964) External heavy-atom spin-orbital coupling effect. V. Absorption studies of triplet states. *J. Chem. Phys.*, **40** (2), 507.

**119** McGlynn, S.P., Azumi, T., and Kinoshita, M. (1969) *Molecular Spectroscopy of the Triplet State*, Prentice-Hall, New Jersey.

**120** Beljonne, D. *et al*. (2001) Spin-orbit coupling and intersystem crossing in conjugated polymers: a configuration interaction description. *J. Phys. Chem. A*, **105** (15), 3899.

**121** Klingshirn, C.F. (1997) *Semiconductor Optics*, Springer-Verlag, Berlin, ISBN: 978-3540583127.

**122** Paus, H.J. (2007) *Physik in Experimenten und Beispielen*, 3rd edn, Hanser-Verlag München, ISBN: 978-3-446-41142-5.

**123** Demtröder, W. (2010) *Atome, Moleküle und Festkörper. Experimentalphysik*, Vol. **Vol. 3**, Springer, Berlin.

**124** Einstein, A. (1917) Zur Quantentheorie der Strahlung. *Phys. Z.*, **18**, 121.

**125** Hilborn, R.C. (1982) Einstein coefficients, cross-sections, F values, dipole-moments, and all that. *Am. J. Phys.*, **50** (11), 982.

**126** Hilborn, R.C. (1983) Correction. *Am. J. Phys.*, **51** (5), 471.

**127** Hilborn, R.C. Einstein coefficients, cross sections, f values, dipole moments, and all that. 2002; Available from: http://arxiv.org/ftp/physics/papers/0202/0202029.pdf.

**128** Robinson, G.W. and Frosch, R.P. (1962) Theory of electronic energy relaxation in solid phase. *J. Chem. Phys.*, **37** (9), 1962.

**129** Robinson, G.W. and Frosch, R.P. (1963) Electronic excitation transfer and relaxation. *J. Chem. Phys.*, **38** (5), 1187.

**130** Siebrand, W. (1966) Mechanism of radiationless triplet decay in aromatic hydrocarbons and magnitude of Franck-Condon factors. *J. Chem. Phys.*, **44** (10), 4055.

**131** Gelbart, W.M., Freed, K.F., and Rice, S.A. (1970) Internal rotation and breakdown of adiabatic approximation - many-phonon Radiationless transitions. *J. Chem. Phys.*, **52** (5), 2460.

**132** Jortner, J., Rice, S.A., and Hochstrasser, R.M. (1969) Raditionless transitions in photochemistry. *Adv. Photochem.*, **7**, 149.

**133** Freed, K.F. and Jortner, J. (1970) Multiphonon processes in nonradiative decay of large molecules. *J. Chem. Phys.*, **52** (12), 6272.

**134** Englman, R. and Jortner, J. (1970) Energy gap law for radiationless transitions in large molecules. *Mol. Phys.*, **18** (2), 145–164.

**135** Craig, D.P. and Ross, I.G. (1954) The triplet triplet absorption spectra of some aromatic hydrocarbons and related substances. *J. Chem. Soc.*, 1589. https://doi.org/10.1039/JR9540001589

**136** Kellogg, R.E. and Schwenker, R.P. (1964) Temperature effect on triplet state lifetimes in solid solutions. *J. Chem. Phys.*, **41** (9), 2860.

**137** Kellogg, R.E. and Bennett, R.G. (1964) Radiationless intermolecular energy transfer. 3. Determination of phosphorescence efficiencies. *J. Chem. Phys.*, **41** (10), 3042.

**138** Lim, E.C. and Laposa, J.D. (1964) Radiationless transitions + deuterium effect on luminescence of some aromatics. *J. Chem. Phys.*, **41** (10), 3257.

**139** Azumi, T. and Mcglynn, S.P. (1963) Delayed fluorescence of solid solutions of Polyacenes. 2. Kinetic considerations. *J. Chem. Phys.*, **39** (5), 1186.

**140** Kellogg, R.E. (1966) Second triplet state of anthracene. *J. Chem. Phys.*, **44** (1), 411.

**141** Hilpern, J.W., Stief, L.J., and Porter, G. (1964) Decay of triplet state. I. First-order processes in solution. *Proc. R. Soc. London, Ser. A: Math. Phys. Sci.*, **277** (1370), 437.

**142** Ermolaev, V.L. (1963) Perenos Energii V Organicheskikh Sistemakh S Uchastiem Tripletnogo Sostoyaniya. 3. Tverdye Rastvory I Kristally. *Usp. Fiziol. Nauk*, **80** (1), 3.

**143** Ermolaev, V.L. (1963) English translation. *Sov. Phys.-Usp.*, **6**, 333.

**144** Kober, E.M. *et al*. (1986) Application of the energy-gap law to excited-state decay of osmium(ii) polypyridine complexes - calculation of relative nonradiative

decay-rates from emission spectral profiles. *J. Phys. Chem.*, **90** (16), 3722.

**145** Browne, W.R. and Vos, J.G. (2001) The effect of deuteriation on the emission lifetime of inorganic compounds. *Coord. Chem. Rev.*, **219**, 761.

**146** Siebrand, W. (1967) Radiationless transitions in polyatomic molecules. 2. Triplet-ground-state transitions in aromatic hydrocarbons. *J. Chem. Phys.*, **47** (7), 2411.

**147** Siebrand, W. and Williams, D.F. (1967) Isotope rule for radiationless transitions with an application to triplet decay in aromatic hydrocarbons. *J. Chem. Phys.*, **46** (1), 403.

**148** Wilson, J.S. *et al.* (2001) The energy gap law for triplet states in Pt-containing conjugated polymers and monomers. *JACS*, **123** (38), 9412–9417.

**149** Beer, M. and Longuethiggins, H.C. (1955) Anomalous light emission of Azulene. *J. Chem. Phys.*, **23** (8), 1390.

**150** Viswanath, G. and Kasha, M. (1956) Confirmation of the anomalous fluorescence of Azulene. *J. Chem. Phys.*, **24** (3), 574.

**151** Sidman, J.W. and Mcclure, D.S. (1956) Electronic and vibrational states of Azulene. *J. Chem. Phys.*, **24** (4), 757.

**152** Ruzevich, Z.S. (1963) Fluorescence and absorption spectra of Azulene in frozen crystalline solutions. *Opt. Spektrosk.*, **15** (3), 357.

**153** Marcus, R.A. (1956) On the theory of oxidation-reduction reactions involving electron transfer. 1. *J. Chem. Phys.*, **24** (5), 966.

**154** Baleizão, C. and Berberan-Santos, M.N. (2007) Thermally activated delayed fluorescence as a cycling process between excited singlet and triplet states: application to the fullerenes. *J. Chem. Phys.*, **126** (20).

**155** Rissler, J. *et al.* (2001) Excited states of ladder-type poly-p-phenylene oligomers. *Phys. Rev. B*, **64** (4), 045122.

**156** Samuel, I.D.W. *et al.* (1993) The efficiency and time-dependence of luminescence from poly(p-phenylene vinylene) and derivatives. *Chem. Phys. Lett.*, **213** (5-6), 472.

**157** Peeters, E. *et al.* (2000) Singlet and triplet excitations of chiral dialkoxy-p-phenylene vinylene oligomers. *J. Chem. Phys.*, **112** (21), 9445–9454.

**158** Ho, P.K.H. *et al.* (2001) Photoluminescence of poly(p-phenylenevinylene)–silica nanocomposites: evidence for dual emission by Franck–Condon analysis. *J. Chem. Phys.*, **115**, 2709.

**159** Romanovskii, Y.V. and Bassler, H. (2000) Phosphorescence from a ladder-type conjugated polymer in solid solutions at low temperature. *Chem. Phys. Lett.*, **326** (1-2), 51.

**160** Hoffmann, S.T. *et al.* (2010) Triplet energy transfer in conjugated polymers. III. An experimental assessment regarding the influence of disorder on polaronic transport. *Phys. Rev. B*, **81** (16), 165208.

**161** Laquai, F. *et al.* (2003) Sensitized intrinsic phosphorescence from a poly(phenylene-vinylene) derivative. *Chem. Phys. Lett.*, **375** (3-4), 286.

**162** Tanaka, I. and Tokito, S. (2007) Energy-transfer processes between phosphorescent guest and fluorescent host molecules in phosphorescent OLEDs. in *Highly efficient OLEDs with Phosphorescent Materials* (ed. H. Yersin), Wiley-VCH, ISBN: 978-3527405947.

**163** Brandrup, J., Immergut, E.H., and Grulke, E.A. (1999) *Polymer Handbook*, 4th edn, John Wiley & Sons, Inc, New York.

**164** Abboud, J.L.M. and Notario, R. (1999) Critical compilation of scales of solvent parameters. Part I. Pure, non-hydrogen bond donor solvents - technical report. *Pure Appl. Chem.*, **71** (4), 645–718.

**165** Vandenburg, H.J. *et al.* (1999) A simple solvent selection method for accelerated solvent extraction of additives from polymers. *Analyst*, **124** (11), 1707–1710.

**166** Grell, M. *et al.* (1998) Chain geometry, solution aggregation and enhanced dichroism in the liquid-crystalline conjugated polymer poly(9,9-dioctylfluorene). *Acta Polym.*, **49** (8), 439–444.

**167** Cossiello, R.F., Akcelrud, L., and Atvars, D.Z. (2005) Solvent and molecular weight effects on fluorescence emission of MEH-PPV. *J. Braz. Chem. Soc.*, **16** (1), 74–86.

**168** Chen, H.C. *et al.* (2009) Full color light-emitting electrospun nanofibers prepared from PFO/MEH-PPV/PMMA ternary blends. *J. Polym. Sci., Part B: Polym. Phys.*, **47** (5), 463–470.

**169** Hansen, C.M. and Hansen Solubility Parameters (2007) *A User's Handbook*, 2nd edn, CRC Press Inc.

**170** deMello, J.C., Wittmann, H.F., and Friend, R.H. (1997) An improved experimental determination of external photoluminescence quantum efficiency. *Adv. Mater.*, **9** (3), 230–232.

**171** Zoppi, L. *et al.* (2008) Defect-induced effects on carrier migration through one-dimensional poly(para-phenylenevinylene) chains. *Phys. Rev. B*, **78**, 165204.

**172** List, E.J.W. *et al.* (2002) The effect of keto defect sites on the emission properties of polyfluorene-type materials. *Adv. Mater.*, **14** (5), 374.

**173** Endo, A. *et al.* (2011) Efficient up-conversion of triplet excitons into a singlet state and its application for organic light emitting diodes. *Appl. Phys. Lett.*, **98** (8), 083302.

**174** Baluschev, S. *et al*. (2006) Up-conversion fluorescence: noncoherent excitation by sunlight. *Phys. Rev. Lett.*, **97** (14), 143903.

**175** Keivanidis, P.E. *et al*. (2011) Electron-exchange-assisted photon energy up-conversion in thin films of pi-conjugated polymeric composites. *J. Phys. Chem. Lett.*, **2** (15), 1893.

**176** Mollay, B. *et al*. (1994) Dynamics of singlet excitations in conjugated polymers - poly(Phenylenevinylene) and poly(Phenylphenylenevinylene). *Phys. Rev. B*, **50** (15), 10769.

**177** Brunner, K. *et al*. (2000) Site torsional motion and dispersive excitation hopping transfer in pi-conjugated polymers. *J. Phys. Chem. B*, **104** (16), 3781.

**178** Herz, L.M. *et al*. (2004) Time-dependent energy transfer rates in a conjugated polymer guest-host system. *Phys. Rev. B*, **70** (16), 165207.

**179** Kelly, D. *et al*. (2022) Laplace transform fitting as a tool to uncover distributions of reverse intersystem crossing rates in TADF systems. *J. Phys. Chem. Lett.*, **13** (30), 6981.

**180** Hildner, R., Streak-Camera-Picture of a MeLPPP-film at room temperature. unpublished.

**181** Wasserberg, D. *et al*. (2005) Comparison of the chain length dependence of the singlet- and triplet-excited states of oligofluorenes. *Chem. Phys. Lett.*, **411** (1-3), 273.

**182** Dellepiane, G. *et al*. (1993) Long-lived photoexcited states in symmetrical polydicarbazolyldiacetylene. *Phys. Rev. B*, **48** (11), 7850.

**183** Cabanillas-Gonzalez, J., Grancini, G., and Lanzani, G. (2011) Pump-probe spectroscopy in organic semiconductors: monitoring fundamental processes of relevance in optoelectronics. *Adv. Mater.*, **23** (46), 5468–5485.

**184** Cerullo, G. *et al*. (1998) Excited-state dynamics of poly(para-phenylene)-type ladder polymers at high photoexcitation density. *Phys. Rev. B*, **57** (20), 12806–12811.

**185** Cabanillas-Gonzalez, J. *et al*. (2005) Photophysics of charge transfer in a polyfluorene/violanthrone blend. *Phys. Rev. B*, **71** (1), 014211.

**186** Kraabel, B. *et al*. (2000) Unified picture of the photoexcitations in phenylene-based conjugated polymers: universal spectral and dynamical features in subpicosecond transient absorption. *Phys. Rev. B*, **61** (12), 8501–8515.

**187** Korovyanko, O.J. *et al*. (2001) Photoexcitation dynamics in regioregular and regiorandom polythiophene films. *Phys. Rev. B*, **64** (23), 235122.

**188** Strobl, G.R. (2007) *The Physics of Polymers*, 3rd edn, Springer, ISBN: 978-3-540-25278-8.

**189** Klessinger, M. and Michl, J. (1995) *Excited States and Photochemistry of Organic Molecules*, VCH Publishers, New York.

**190** Hollas, J.M. (2008) *Modern Spectroscopy*, 4th edn, J. Wiley & Sons, Chicester, ISBN: 978-0-470-84416-8.

**191** Lakowicz, J.R. (1999) *Principles of Fluorescence Spectroscopy*, 1nd edn, Kluwer, Academic/Plenum Publishers, New York.

**192** Valeur, B. (2002) *Molecular Fluorescence*, Wiley-VCH, Weinheim, ISBN: 978-3-527-29929-5.